Additively Manufactured Low-frequency Piezoelectric Energy Harvester Design: Modeling, Fabrication, And Experiment

by

Minh Hao Dinh

A thesis
presented to the University of Waterloo
in fulfillment of the
thesis requirement for the degree of
Master of Applied Science
in
Mechanical and Mechatronics Engineering

Waterloo, Ontario, Canada, 2024

Author's Declaration

I hereby declare that I am the sole author of this thesis. This is a true copy of the thesis, including any required final revisions, as accepted by my examiners.

I understand that my thesis may be made electronically available to the public.

Abstract

With conventional energy sources like fossil fuels becoming increasingly scarce and the widespread adoption of electric vehicles placing growing demands on lithium, the primary material in battery manufacturing, there is a critical need for scientists and engineers to explore alternative energy sources for powering microelectronic devices. Among these alternatives, integrating piezoelectric materials within cantilever beam structures for energy harvesting applications is a promising solution, attributed to its straightforward design and ability to undergo significant deformation under applied loads.

However, this technological approach faces notable challenges, including limitations associated with low power density and a high natural frequency due to inherent geometric constraints. These challenges have become a focal point for ongoing research endeavours to enhance the efficiency and applicability of piezoelectric energy harvesting. This thesis delves into a prospective solution for powering microelectronic devices, emphasizing its merits in terms of uncomplicated packaging and advancements in micro-scale power density. A MEMS ring-shaped piezoelectric energy harvesting device was fabricated, utilizing 3D printing for substrate production and precision dicing techniques to achieve the required dimensions of the piezoelectric material. The device's design was modelled using SOLIDWORKS, and its performance was thoroughly simulated in COMSOL to ensure alignment with observations.

Inspired by the Vesper microphone's square form, the energy harvester's geometric configuration offers scalability and the potential for incorporating multiple cantilever beams. According to the findings, this energy harvester demonstrates a total power output of 53.46 μW when subjected to an acceleration of 0.08g, establishing its promising viability relative to other energy harvesting technologies. The study presents a novel approach to energy harvesting and highlights the practical implications and potential advancements in micro-scale power generation for sustainable electronic devices.

Acknowledgments

Table of Contents

List of Figures

List of Tables

Chapter 1

Introduction

1.1 Motivation

In pursuing economic growth, undertaking various infrastructure projects encompassing the construction of buildings, bridges, and power grids becomes imperative to accommodate the expanding population. To manage and maintain these infrastructures, it is paramount to collect and transmit various environmental data, including temperature, humidity, atmospheric acidity, and local vibrations [1]. These data provide comprehensive insight into structural health. Therefore, it is critical to establish and deploy wireless sensor networks (WSN) urgently because WSNs, strategically deployed in remote or challenging-to-access locations, play a pivotal role in capturing, storing, and transmitting physical or environmental data from their surroundings [2]. They are deemed extremely essential and play an important role in maintaining the structural integrity of critical infrastructure, enhancing its longevity, and ensuring public safety [3].

Despite the importance of WSN, the reliance of WSN on batteries for normal operations presents a significant predicament, especially considering the difficulty of accessing deployment sites and the associated escalating costs. Moreover, the booming growth in the electric vehicle manufacturing sector further exacerbates the situation, leading to a shortage of lithium, a primary component in battery production [4] while the finite lifespan of lithium batteries, susceptible to harsh environmental conditions such as temperature and humidity, results in a shorter lifespan than WSNs. In addition, the power line must be disconnected to facilitate the installation of specific current sensors, which may introduce

disruptions within the designated area [5]. Consequently, it is necessary to engineer a solution for the WSN that minimizes such disturbances. This solution should be characterized by ease of implementation, cost-effectiveness, and autonomous operation.

In response to these challenges, researchers actively explore alternative solutions to replace traditional lithium batteries. Among the viable alternatives, mechanical vibration-based energy harvesting technology using Piezoelectric material emerges as one of the most effective choices [6]. This technology seeks to directly convert kinetic ambient energy from the environment into usable electrical energy. Figure 1.1 [7] illustrates the schematic representation of the energy harvesting system incorporated into a sensor. Kinetic energy is ubiquitous and available everywhere; therefore, it can be harnessed and converted into valuable electrical energy [6].
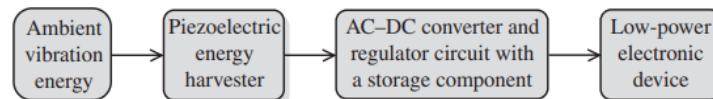
Figure 1.1: Schematic representation of the application concept of a piezoelectric energy harvesting system

One of the primary advantages of this technology over traditional batteries is its cleanliness and longevity. While batteries pose significant challenges for recycling at the end of their life cycle [8], a well-designed Piezoelectric (PZT) energy harvester can operate indefinitely. However, specific challenges impede the seamless implementation of this technology into WSN, such as low power density and high natural frequency resulting from the brittleness of the piezoelectric material and size constraints of the WSN [2]. This thesis introduces a piezoelectric energy harvester design featuring 6 independent energy harvester units. This design aims to enhance operational flexibility and increase power output. The geometry is characterized by a low natural frequency and minimal strain nodes, contributing to its effectiveness. Additive manufacturing is emphasized for rapid prototyping and achieving complex geometries in a compact size. The feasibility of utilizing additively manufactured substrates to support the deployment of the compact energy harvesting unit. The thesis presents promising results, showing power spectral densities comparable to other researchers. Furthermore, a comparative analysis with existing proposals from the literature will be provided to highlight the inherent advantages of this design.

1.2 Scope of Research

The central objective of this master's thesis is to establish a sustainable energy source solution tailored for sensor networks. In pursuit of this goal, the research proposes the development of a sophisticated, multi-body structured energy harvester. This envisioned model incorporates intricate irregular shapes, achieved through advanced 3D printing techniques, with the explicit purpose of reducing the natural frequency of the entire system to a critical operational threshold below 100 Hz. This threshold is significant for effectively integrating the energy harvester into various residential and industrial systems, as documented in [9]. Moreover, the design focuses on adhering to size limitations, ensuring the viability of incorporation into small-scale power electronic devices.

The research methodology involves establishing well-defined design criteria, which leads to constructing a finite element model (FEA) within the COMSOL software. This computational model predicts the system's mechanical and electrical characteristics during vibrational conditions. The insights from the FEA inform design optimization, encompassing operating conditions, geometric considerations, and manufacturing feasibility.

Upon completing the design and simulation phase, the research advances to fabricating a physical prototype. This prototype is fabricated using state-of-the-art 3D metal additive manufacturing techniques and advanced piezoelectric (PZT) materials fabrication processes. Subsequently, experimental testing is conducted, employing base excitation methods to subject the prototype structure to vibrational forces. The resulting experimental data is meticulously compared and validated against the computer simulation model, facilitating corrections and updates to refine the overall design.

Additionally, the research focuses on identifying the optimal resistance load for the energy harvesting system through an experimental approach. This exploration is essential for enhancing the overall efficiency and performance of the developed energy harvester. Through a comprehensive and iterative process involving design, simulation, fabrication, and experimentation, this research aims to contribute significantly to sustainable energy solutions tailored explicitly for sensor networks.

1.3 Contribution

Previous research explored the viability of mechanical vibration energy harvesters as an energy source for small-scale electronic devices. This thesis introduces a novel design that goes beyond the conventional, offering a structure designed to scale power output during operation while maintaining a low natural frequency within a compact footprint. The innovative approach taken in this research aims to address existing designs' limitations and enhance energy harvesting systems' efficiency.

Moreover, the fabrication process incorporates cutting-edge 3D additive manufacturing techniques to bring the proposed design to life in the physical realm. This advanced manufacturing approach allows the energy harvester to possess an irregular shape, a feature typically impractical with traditional methods. The distinctive shape plays a crucial role in lowering the device's fundamental natural frequency, aligning with the operational requirements for small-scale electronic devices. This aspect sets the presented design apart, showcasing a commitment to innovation and pushing the technological boundaries by employing advanced manufacturing techniques.

1.4 Thesis Outline

The thesis is outlined in the following structure:

Chapter 2: Literature Review

Chapter 2 introduces energy harvesting technology to establish a comprehensive understanding of the underlying theories and mathematical models associated with the cantilever beam structure and the mechanical-to-electrical conversion model of piezoelectric materials. By exploring the foundational principles, readers will gain insight into the intricate mechanics that govern energy harvesting processes. Additionally, the chapter provides a concise overview of recent developments in piezoelectric energy harvesters. This review of cutting-edge advancements aims to enhance comprehension of the technology's strengths and limitations, offering a broader context for the subsequent chapters.

Moreover, Chapter 2 offers a detailed preview of the energy harvesting fabrication process, emphasizing critical aspects such as substrate and PZT fabrication. By introducing the intricacies of the fabrication process, this chapter presents a robust foundation for understanding the practical aspects of implementing energy harvesting technologies.

Chapter 3: PZT Energy Harvester Modelling, Design and Simulation

Building on the theoretical foundations established in Chapter 2, Chapter 3 presents a detailed examination of the design criteria, incorporating limitations and operational frequencies. The chapter introduces the initial design concept, offering an insight into the creative process that precedes the development of a sophisticated energy harvester.

The ultimate design is unveiled in this chapter, complete with detailed illustrations and a selection of materials. The chapter further explores the concept of strain matching, providing a necessary understanding of the mechanical intricacies that contribute to the overall effectiveness of the energy harvester. An integral component of Chapter 3 is introducing a Finite Element Analysis (FEA) model. Based on the 3D model from SOLIDWORKS, the computational model developed in COMSOL facilitates in-depth analysis of critical parameters, including geometry and the mechanical and electrical properties of the substrate and the piezoelectric material.

Chapter 4: Fabrication, Experimental Procedure, Result and Validation

Chapter 4 delves into the practical implementation of the proposed design, detailing the fabrication procedure for the substrate through advanced 3D printing techniques. Incorporating a heat treatment phase is highlighted as a crucial step in augmenting the mechanical characteristics of the substrate, showcasing the attention to detail in the fabrication process. The chapter further introduces the fabrication process for the Piezoelectric material.

Following the fabrication, Chapter 4 introduces the experimental methodology, comprehensively describing the setup. This section bridges theory and practice by outlining the steps to validate the theoretical models through empirical testing. The chapter concludes by thoroughly discussing the empirical findings and drawing comparisons against the FEA model. Voltage and power calculations are presented. Additionally, the determination of the optimal resistance for the structure is addressed, further enriching the practical insights derived from the experimental analysis.

Chapter 5: Conclusion

The final chapter, Chapter 5, offers a comprehensive conclusion drawn from the research findings, emphasizing the contributions made to energy harvesting. Beyond a mere summary, the chapter provides insightful reflections on the implications of the research, contributing to the broader discourse on sustainable energy solutions.

Furthermore, Chapter 5 recommends potential enhancements to the design in the future. This forward-looking perspective positions the research within the context of ongoing advancements in the field, inviting further exploration and innovation. By offering practical insights and suggesting avenues for future research, this chapter extends the impact of the thesis beyond its immediate scope.

Chapter 2

Literature Review

2.1 Piezoelectric Energy Harvester

A spectrum of energy harvesting methods has been proposed, encompassing electromagnetic, electrostatic, piezoelectric (PZT), triboelectric, thermoelectric, and pyroelectric transduction mechanisms [10]. Among these diverse options, the PZT energy harvester emerges as a favoured choice, primarily due to its remarkable ability to efficiently convert mechanical strain into electrical energy. Notably, the PZT energy harvester achieves this attribute without requiring additional external sources, such as a separate voltage source, magnetic field, or contact with another material, as seen in electrostatic, electromagnetic, and triboelectric energy harvesting [10]. This intrinsic self-sufficiency contributes to the appeal of PZT energy harvesting, making it an attractive solution in the quest for sustainable energy.

Furthermore, the versatility of PZT devices is underscored by their feasibility of fabrication at both macro-scale and micro-scale. This flexibility is made possible through thick-film and thin-film fabrication techniques, setting PZT apart from electromagnetic devices that may face limitations in miniaturization. This capability to produce PZT devices at different scales opens up avenues for diverse applications across various sectors, aligning with the imperative of energy harvesting solutions that are adaptable and scalable to different contexts [7]. As researchers explore deeper into optimizing and expanding the capabilities of PZT energy harvesters, their potential contribution to sustainable energy solutions becomes increasingly promising.

2.1.1 Piezoelectric Material

PZT materials, distinguished by their remarkable electromechanical coupling properties, exhibit a fascinating dual-action behaviour known as the direct PZT effect. This effect, originating from the crystalline structure of PZT materials, allows them to generate electrical potential when subjected to external forces that induce mechanical stress within the material, leading to the separation of positive and negative charges within the material and resulting in electric voltage output. In addition, PZT materials also display the inverse PZT effect, wherein they undergo deformation when exposed to an applied electric field, showcasing their versatility in sensing and actuation applications [11].

The dual-action behaviour of PZT materials makes them indispensable for various applications requiring high accuracy and precision. These applications span a broad spectrum, including medical diagnostics through ultrasound imaging, precision motion control in robotics, and energy harvesting from ambient vibrations for powering electronic devices. Their unique electromechanical properties underscore the profound significance of PZT materials in modern technology and innovation [12–14].

Within the PZT materials family, ceramic materials have emerged as the preferred choice due to their compelling affordability, stability, and exceptional PZT performance. Recent research has highlighted the prominence of ceramic materials, particularly Lead Zirconate Titanate (PZT), Potassium Sodium Niobate (KNN), and Aluminum Nitride (AlN), among others [15]. PZT, in particular, stands out as an ideal choice for efficiently converting mechanical energy into electrical energy, especially in energy harvesting applications.

Recent studies further support the PZT's resilience in harsh environmental conditions, ensuring long-term durability and reliability [15]. The cost-effectiveness of ceramic materials, including PZT, adds to their appeal and facilitates their widespread adoption in diverse applications related to sustainable energy solutions [16, 17]. This positions PZT materials, particularly ceramics like PZT, as a leading preference for applications demanding reliability, efficiency, and cost-effectiveness in the ever-evolving landscape of technology and innovation.

2.1.2   Cantilever Beam Energy Harvester

Energy harvesting systems commonly rely on a specific design known as the cantilever beam, as illustrated in Figure 2.1 [7], without clamps. This design offers several key advantages, making it a preferred choice in various applications. The cantilever beam's notable benefits include its ability to produce large deformation under significant tension and compression, its simplicity in terms of manufacturing, and its natural tendency to operate at a low frequency [18].
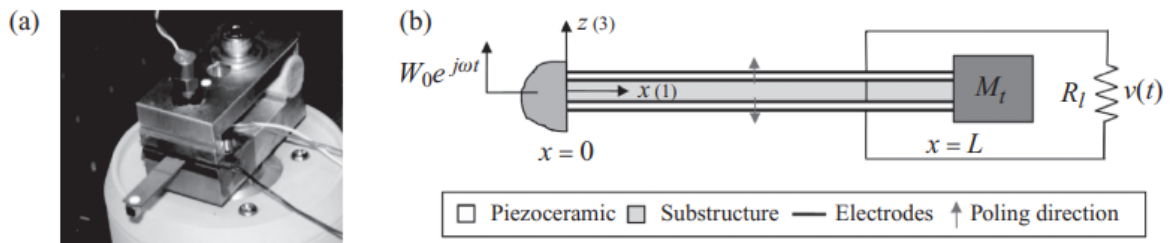
Figure 2.1: (a) A cantilevered PZT energy harvester tested under base excitation and (b) its schematic representation

Typically, the cantilever beam is constructed in two primary ways. The first involves using just two layers, where one layer consists of PZT material, and the other is a substrate, known as unimorph configuration. The second approach employs three layers, with PZT layers sandwiching a substrate layer, known as bimorph configuration [10].

A pivotal element in the cantilever beam design is incorporating a tip mass at the end of the beam. This component is crucial in tuning the beam's natural frequency to align with the target energy source's frequency. This synchronization is vital for optimizing the energy harvesting system and maximizing power output. Therefore, the accurate selection and adjustment of the tip mass are critical factors in designing and optimizing these energy-harvesting setups. The effectiveness of the entire system hinges on the careful consideration and fine-tuning of this crucial component.
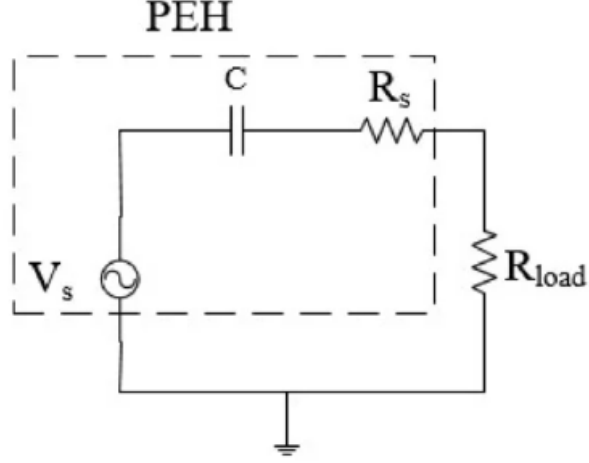
Figure 2.2: Equivalent circuit for a PZT energy harvesting

In addition, the PZT energy harvester can be represented as an electrical configuration. Capacitors and resistors play integral roles in this setup, as illustrated in Figure 2.2 [19]. A resistor is expressly incorporated into the system to quantify the power generated by the energy harvester [5]. This resistor is strategically included to measure and analyze the output power of the energy harvesting system, providing valuable insights into its performance characteristics.
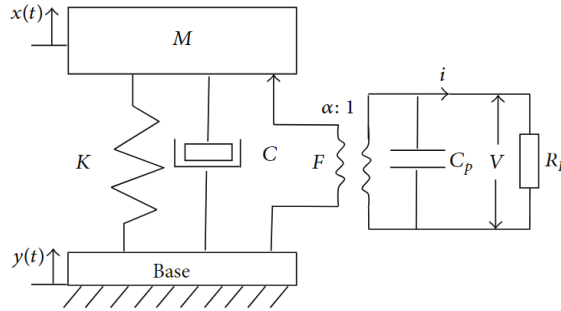
Figure 2.3: Lumped parameter models for the PZT cantilever beam

The PZT cantilever beam can also be modelled as a single degree of freedom (SDOF) as illustrated in Figure 2.3 [20], and the response of the system can be obtained per the equation below [21]:

$$z(t) = \frac{\omega^2 m_{\text{eq}}}{k_{\text{eq}} - \omega^2 m_{\text{eq}} + i\omega c_{\text{eq}}} Y_0 e^{i\omega t} \tag{2.1}$$

In the context, where $z(t) = x(t) - y(t)$ represents the displacement of the mass relative to the base, it can be defined by the equivalent stiffness, mass, and damping of the beam

10

as follows: $k_{\text{eq}} = 3EI/L^3, m_{\text{eq}} = 33/140mL + M_t$ (where M_{t} denotes the tip mass) and $c_{\text{eq}} = 2\zeta\omega_n m_{\text{eq}}$ with ζ representing the equivalent damping ratio[21]. Additionally, Y_0 represents the amplitude of the excitation, and ω is the input angular frequency. The natural frequency of the system (ω_n) can be calculated using the following equation:

$$\omega_n = \sqrt{k_{\text{eq}}/m_{\text{eq}}} \tag{2.2}$$

2.2 Low-Frequency Energy Harvester

Integrating the PZT energy harvester into the micro-scale sensor networks presents intricate design challenges. As the micro size of sensor network components drives the need for compactness, the energy harvesting system exhibits a substantially higher natural frequency than the ambient vibrations it seeks to harness. Reilly *et al.* 's research indicates that most ambient vibration sources in various environments, including residential and commercial spaces, are characterized by frequencies below 100 Hz [9]. However, as reported in the earlier literature, the energy harvester was designed in the kHz range due to the high thickness-to-length ratio for MEMS devices [22]. Consequently, the mismatch between the system's natural and source frequencies leads to insufficient power generation to sustain the sensors. Traditional techniques employed to lower the natural frequency of a cantilever beam system encompass:

- Increasing the tip mass.

- Reducing the substrate thickness.

- Extending the beam length.

Even though increasing the tip mass and reducing the substrate thickness can effectively reduce the natural frequency, due to the size constraint of the WSN devices and fabrication techniques, these methods are limited to significantly impacting the natural frequency. Therefore, researchers have focused on increasing the beam length by devising various energy harvester geometry designs to address this challenge. Reviewing these cutting-edge developments in this section will help comprehensively analyze and identify their pros and cons.

Furthermore, with this extensive review and analysis, the next part of the thesis introduces the proposed design. This design incorporates the lessons learned and advantages gained from previous research. Doing so aims to open a new course that effectively tackles the energy harvesting challenges in WSN. Ultimately, the goal is to contribute to a more sustainable and cost-effective future.

2.2.1 Zigzag Design

Karami and Inman have proposed a solution to mitigate the challenge posed by high resonant frequencies in microelectromechanical (MEMS) energy harvesting, representing a significant contribution to the field. The innovative design introduces a complex zigzag structure that interconnects multiple beams through link portions situated at their endpoints, as visually depicted in Figure 2.4 [22–25]. This intricate structural configuration consists of two distinct layers: one incorporating the substrate and the other comprising the PZT material. Additionally, incorporating a tip mass strategically attached to the end of each beam allows for precise frequency tuning, thereby optimizing the energy conversion process [22].
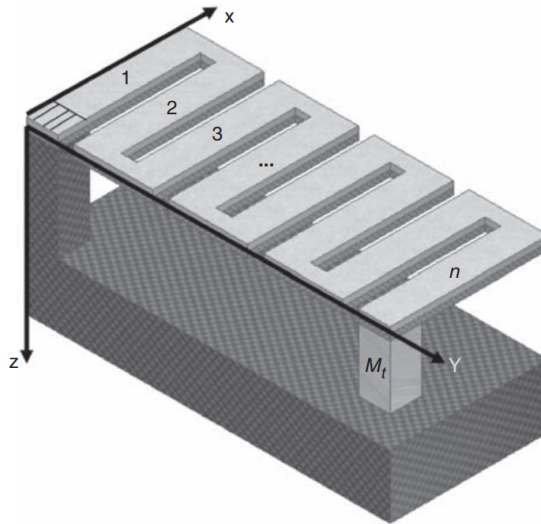
Figure 2.4: The zigzag energy-harvesting structure

Karami's comprehensive research findings demonstrate that the nine-member zigzag structure exhibits a remarkable 2.5-fold increase in maximum power generation compared to a conventional single-beam setup [22]. However, this enhancement in power output brings forth a consideration that catches careful attention. As additional members are introduced to the zigzag structure, it becomes increasingly susceptible to torsional vibration modes, potentially impacting power output. The presence of these modes introduces challenges such as charge cancellation due to variations in strain nodes [22]. Consequently, the engineering decision regarding the number of members within the structure becomes pivotal, demanding a delicate balance to fully exploit the potential of energy harvesting

while effectively managing the effects of unwanted vibrations.

This breakthrough design showcases a substantial improvement in power generation and underscores the need to optimize the structural configuration for practical applications. The findings from this research hold immense promise for advancing the realm of MEMS energy harvesting technology. The intricate design and the associated considerations emphasize optimizing to harness this innovative solution's full potential, which marks significant progress in pursuing efficient and effective energy harvesting methodologies for MEMS devices.

2.2.2 Elephant Design

The introduction of the torsionally dominant zigzag shape marked a significant milestone in energy harvesting technology, prompting sustained research efforts to refine and optimize this unique configuration. Building upon the foundation laid by the zigzag design, a proposal for further enhancing its capabilities has emerged in the form of the "Elephant" design. This approach, researched by Sharpes *et al.* and visually shown in Figure 2.5 [26], presents a compelling solution to address the inherent torsional effects associated with the traditional zigzag design, all while maintaining a compact footprint and a low natural frequency.
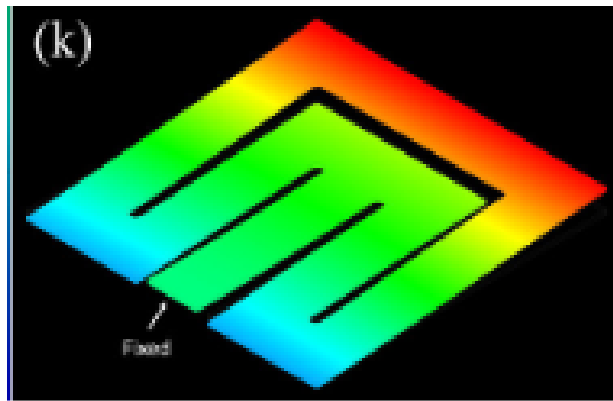
Figure 2.5: The elephant zigzag energy-harvesting structure

The symmetrical attribute of the design offers a distinct advantage by promoting a more pronounced occurrence of pure bending during the excitation process. This characteristic leads to heightened stress concentration within the structure, resulting in a considerable increase in power generation compared to the conventional zigzag design [26].

14

Moreover, the elephant harvester's standout feature lies in its practical beam tip, which can accommodate a substantial tip mass without compromising its fundamental low-profile configuration [26]. This innovative design addresses the challenges posed by torsional effects and showcases a significant advancement in power generation efficiency, offering a promising avenue for the evolution of energy harvesting technology. The Elephant design's unique attributes contribute to its potential applicability in diverse scenarios, emphasizing the importance of continued exploration and refinement in the quest for optimal energy harvesting solutions.

2.2.3   Folded Design

The folded design introduced by Bath *et al.* is presented in Figure 2.6 [2]. The design is inspired by the symmetrical zigzag shape of the elephant design, this configuration incorporates an additional substrate layer to optimize the footprint further [2]. This addition enhances the effective PZT area, improving energy harvesting potential. However, it is crucial to acknowledge certain limitations associated with this design.
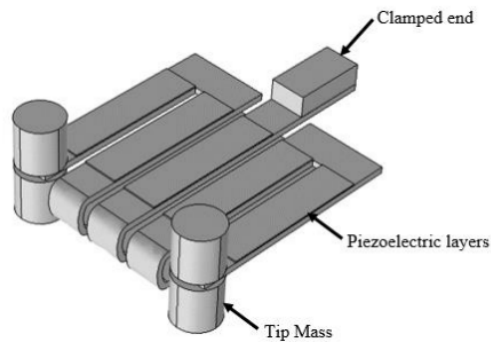
Figure 2.6: The folded energy-harvesting structure

One drawback lies in the thickness of the substrate, which, when increased, leads to a subsequent rise in the structure's natural frequency. Additionally, the utilization of bulk PZT materials (0.191mm) contributes to the stiffness of the overall structure, further increasing its natural frequency. Four tip masses were introduced to address these challenges. This strategic addition aims to fine-tune the structure's natural frequency to fall below 100 Hz to keep it suitable for harvesting energy from low-frequency ambient sources. Despite this

optimization effort, it is essential to recognize that the structure, while achieving the desired natural frequency, becomes bulkier, presenting challenges in integration into Wireless Sensor Networks (WSN).

The trade-offs in the folded design underscore the balance between achieving optimal energy harvesting performance and practical considerations for seamless integration into real-world applications. This design contributes to the overall landscape of energy harvesting technologies, emphasizing the ongoing need for innovative solutions that navigate the complex interplay of design parameters and application requirements.

2.2.4 Spiral Design

Initially explored by Brewer [27], the spiral design features a cantilever beam geometry tailored to meet size and natural frequency requirements. Similar to a one-dimensional cantilever beam, its resonant frequency is linked to its total length. Additionally, variations in the width affect the natural frequency of the spiral design, unlike the one-dimensional cantilever beam [27]. Ibrahim *et al.* utilized this design for PZT energy harvesting from electromagnetic sources, aiming to achieve a low natural frequency of 21 Hz [28]. Figure 2.7 [28] shows the finite element analysis (FEA) model of the spiral beam geometry used for analyzing its dynamics and power output.
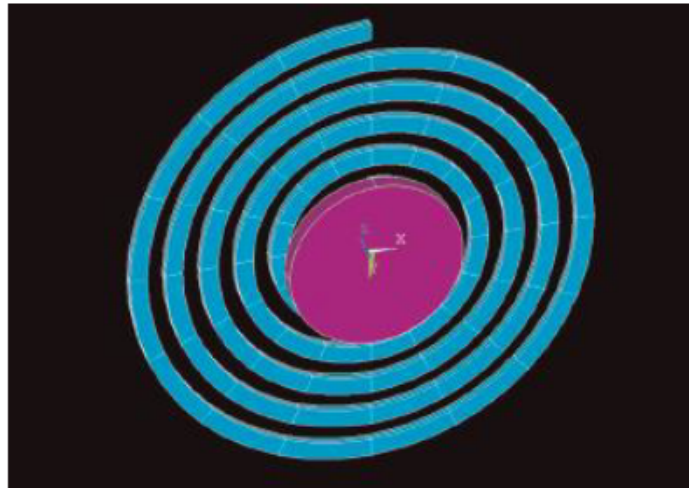
Figure 2.7: Piezomagnet harvester encompassing a spiral piezoelectric bimorph and a magnet attached to the center of the spiral.

The study by Karami *et al.* delves into the analysis of the geometry of a design involving

spiral vibrations, determining them to be torsional [29]. This characterization leads to the conclusion that the complex design pattern of the PZT material is required to be attached to the spiral substrate. Despite achieving the design objective of attaining a low natural frequency within a compact footprint, torsional vibration in its first natural frequency limits its applicability in energy harvesting applications.

2.3   Fabrication

This section thoroughly establishes the knowledge that forms the basis for fabricating the energy harvesting structure outlined in this thesis. The comprehensive review explores various vital aspects, encompassing the substrate fabrication method, subsequent post-processing techniques applied to the substrate, and the processing method employed for the piezoelectric material. Each of these components plays a pivotal role in shaping the structure's functionality and performance, and a detailed examination of their underlying principles is essential for understanding the energy harvesting system's complexity. The insights garnered from this comprehensive review lay the groundwork for the subsequent discussions and analyses, contributing to a robust framework for evaluating and interpreting the experimental findings presented in the later sections of this thesis.

2.3.1   Metal Additive Manufacturing

Additive Manufacturing (AM), commonly known as 3D printing, signifies a shift in contemporary manufacturing by facilitating the direct transformation of intricate 3D computer-aided design (CAD) models into tangible physical objects. This groundbreaking technology employs a systematic layer-by-layer approach, deconstructing 3D models into numerous discrete slices, each successively printed atop the other. AM utilizes various materials, showcasing impressive versatility and adaptability in material selection and application [30].
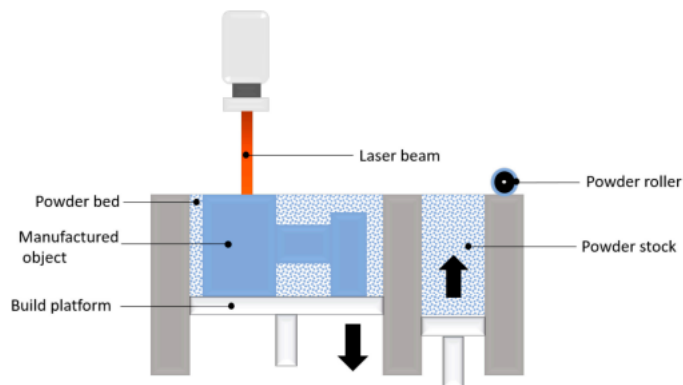
Figure 2.8: Schematic representation of PBF

The transformative potential of AM extends beyond traditional manufacturing constraints, offering solutions to persistent challenges such as material waste and the fabrication of products with intricate and unconventional geometries [31]. Among the various AM techniques, the Powder Bed Fusion (PBF)-based process is a noteworthy example. This technique leverages a concentrated thermal energy source, often in the form of a laser, orchestrating the precise fusion of individual layers of metals into a cohesive, constructed component. The intricate nature of this technology unfolds on the surface of a powdered bed, with each layer meticulously fused to bring forth the final product [30], as exemplified in Figure 2.8 [31].

The advanced technology and innovative engineering inherent in PBF and similar AM methodologies have successfully challenged the limitations of traditional manufacturing, ushering in a new era of limitless possibilities in product design and fabrication. This exploration of AM sets the stage for understanding its pivotal role in the fabrication processes associated with the energy harvesting structure discussed in subsequent sections.

2.3.2   Wafer dicing machining

The dicing technique, a staple in semiconductor manufacturing, emerges as a cornerstone for enhancing efficiency in producing Micro-Electro-Mechanical Systems (MEMS) devices. This method offers a distinct advantage by facilitating the processing of numerous MEMS devices on a single semiconductor wafer, contributing to an optimized semiconductor production workflow. In contrast to conventional subtractive machining approaches, such as laser, electrochemical, and waterjet methods, which often result in undesirable consequences such as excessive chipping and cracking during the machining operation, the dicing technique proves to be a preferred choice for semiconductor device fabrication [32]. Distinguished by its versatility, the dicing technique encompasses various methods tailored to specific applications and requirements within the semiconductor industry, including diamond scribing, laser scribing, and the particularly noteworthy blade dicing method [32].
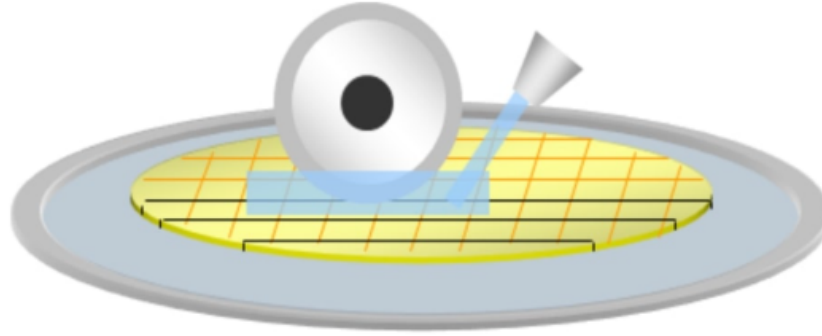
Figure 2.9: Schematic representation of dicing process

Blade dicing, or mechanical dicing as presented in Figure 2.9 [33], stands out prominently because precision and accuracy are paramount in semiconductor manufacturing. The method employs a high-speed rotating blade coated with an abrasive material, typically composed of diamond particles; it allows for the intricate shaping of materials like PZT into small rectangles or squares with exceptional precision and accuracy [32]. The versatility of blade dicing is further underscored by its ability to accommodate a broad spectrum of semiconductor materials, showcasing compatibility with various substances utilized in semiconductor manufacturing. Additionally, the adaptability of blade dicing extends to wafers characterized by varying dimensions, sizes, and thicknesses, emphasizing its efficacy within the semiconductor fabrication domain [34].

Chapter 3

PZT Energy Harvester Modelling, Design and Simulation

3.1 Piezoelectric modelling

In the previous section, the cantilever beam is considered as the most suitable option for the PZT energy harvesting application, highlighting its importance in the discussed design context. The primary mode of operation for the PZT materials on the energy harvester unit is the 31 operating mode. This terminology denotes a specific stress alignment and strain distribution within the structure, predominantly occurring in the 1 direction due to the applied force. Concurrently, an electric field is induced in the 3 direction [11], as shown in figure 3.1. This directional alignment explains the fundamental operational characteristics of the cantilever beam in the proposed energy harvester, offering valuable insights into its behavior and performance.
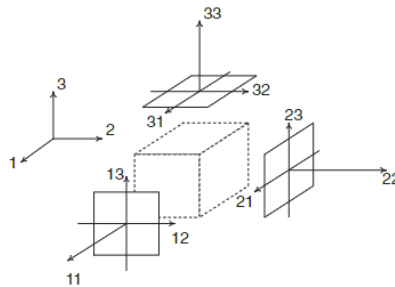
Figure 3.1: Piezoelectric cube indicating the coordinate axes of the three-dimensional analysis.

The foundational equations that establish the correlation between the induced electrical charge within the PZT material and the applied strain are encapsulated by the following constitutive equations:

$$\underline{S} = \mathbf{s}^{E}\underline{T} + \mathbf{d}'\underline{E}$$
$$\underline{D} = \mathbf{d}\underline{T} + \varepsilon^{T}\underline{E},$$

(3.1)

Where S is a 1×6 vector of the induced strain, T is a 1×6 vector of the external stress applied to the material, E is a 1×3 vector of the electric field, D is a 1×3 matrix of the electrical displacement, $\mathbf{s}^{E}$ is a 6×6 matrix of compliance coefficients, d is a 3×6 matrix of piezoelectric strain coefficients, and ε^{T} is a 3×3 matrix of dielectric permittivity values.

Because the 31 mode is the predominant operational mode, the general piezoelectric constitutive equations can be simplified into the strain-charge formulation, as outlined in the following equations:

$$S_1 = s_1^{E}T_1 + d_{13}E_3$$
$$D_3 = d_{13}\ T_1 + \varepsilon_{33}^{T}E_3.$$

(3.2)

3.2 Design Consideration

3.2.1 Piezoelectric Ceramic Types

Numerous options exist for PZT ceramic materials, each tailored to specific applications. However, when the requirement involves high sensitivity, PZT-5A, PZT-5H, and PZT-5J emerge as the favoured choices. In energy harvesting, a crucial aspect is aligning the harvester's frequency with the natural frequency of the host structure. Consequently, selecting a PZT ceramic material for energy harvesting applications places significant emphasis on high sensitivity.

In evaluating harvesting capabilities among these materials, the PZT coupling coefficient (d_{31}) is the primary metric guiding the selection process. This coefficient quantifies the effectiveness of the material in converting kinetic energy into electrical energy in the 31 direction as explained in the previous section. Table 3.1 comprehensively compares the coupling coefficients for PZT-5A, PZT-5H, and PZT-5J [35].

Table 3.1: PZT coefficient for 31 mode

	PZT-5A	PZT-5J	PZT-5H
d_{31} (C/N $\times 10^{-10}$)	-1.9	-2.7	-3.2

As presented in table 3.1, it is shown that PZT-5H possesses the highest absolute coupling coefficient among the materials. However, it is crucial to recognize a limitation associated with PZT-5H, namely its reduced performance at elevated temperatures [35]. When temperatures exceed the Curie temperature threshold, set at 150°C, PZT-5H declines its electrical characteristics. Consequently, it becomes imperative to ensure that the operating temperature of PZT-5H remains well below the Curie temperature, as elaborated in [36].

In the context of this paper, a fundamental assumption is made regarding the environmental temperature at which the PZT sensor operates, implying that it will not surpass 60°C. This assumption aligns with the primary intent of utilizing the sensor for infrastructure health monitoring, where the expected operating conditions remain within the specified temperature range. This consideration is pivotal in optimizing the performance

and longevity of the PZT-5H sensor in practical applications on monitoring and ensuring the structural integrity of infrastructure.

3.2.2 Substrate Material

In energy harvesting, where the demand for effective operation at low frequencies is paramount, the substrate material is a significant design factor, requiring specific characteristics to ensure optimal functionality. A critical consideration in this context is Young's modulus, the depreciation of which becomes imperative to restrict any unwarranted addition of stiffness to the overall structure. Beyond mere structural integrity, the substrate material must also have electrical conductivity, serving a dual purpose as a foundational structural element and the essential ground electrode within the circuit.

Following a thorough review of materials from the Multi-Scale Additive Manufacturing Lab at the University of Waterloo, EOS's 17-4PH powder was selected to fabricate the substrate. This decision is primarily anchored in its low Young's modulus (197 GPa) [37], complemented by elongation at a break of 19.9% [38], and its advantageous low hardness, indicative of a ductile nature. The intrinsic ductility factor ensures heightened durability, particularly under cyclic loading conditions, contributing to the material's resilience and prolonged performance lifespan.

Furthermore, the versatility of the chosen material extends to its potential for substantial enhancement through heat treatment, a process known to yield significant improvements in its mechanical properties [39]. This deliberate and considered selection aligns seamlessly with the distinctive and demanding requirements of energy harvesting. It ensures the substrate meets and exceeds the targeted harvesting specifications, establishing a robust foundation that guarantees optimal performance.

3.2.3 Geometry Design

Developing and optimizing geometric design criteria in energy harvester design is a fundamental pillar, significantly influencing the system's natural frequency. Researchers have developed various methodologies to optimize design in response to the challenge posed by high natural frequencies. These approaches encompass various strategies, including thin-

ning the substrate, introducing tip mass, and extending the cantilever beam structure. A comprehensive review of the literature dedicated to this area reveals a diverse landscape of geometrical configurations, each offering unique solutions to this complex problem.

Among these configurations, the 2D elephant zigzag shape stands out for its ability to lower the natural frequency. This characteristic stems from the elongated beam structure inherent in the zigzag shape and its tendency towards bending-dominant behaviour. However, the effectiveness of this shape is intricately linked to the specific number of beams incorporated into the design, adding a layer of complexity to the optimization process.

The following section will provide a detailed examination of a structural arrangement that transcends the boundaries of a single harvester. The approach involves integrating multiple energy harvesters to amplify the harvested power output. This thorough exploration will illuminate the new strategies and methodologies to enhance energy harvester geometry design.

3.3   Design, Modelling and Simulation

3.3.1   Design

The proposed energy harvester design draws inspiration from the Vesper VM100 MEMS microphone product from Vesper—a commercial PZT MEMS microphone illustrated in figure 3.2 [40]. This design philosophy serves as the guidance for shaping an innovative energy harvester with multiple units.
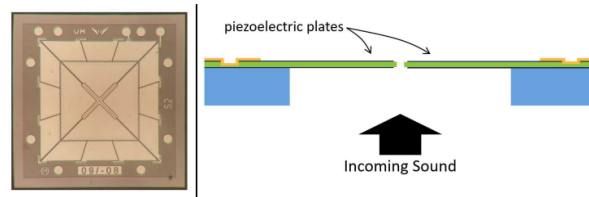
Figure 3.2: Top-view (left) and cross-sectional drawing (right) of Vesper piezoelectric MEMS microphone.

Central to the core of the Vesper design are four strategically positioned PZT triangular cantilever beams to optimize the interaction area with the applied force. Embracing the same design, the PZT energy harvester, made from 17-4PH stainless steel, boasts the incorporation of six two-dimensional zigzag elephant-inspired energy harvesters. These designed harvesters are arranged evenly in a circular pattern, connected to a rim structure as a solid body, as illustrated in figure 3.3. The design's symmetrical configuration aims to ensure an equitable distribution of forces, thereby maximizing energy harvesting efficiency.
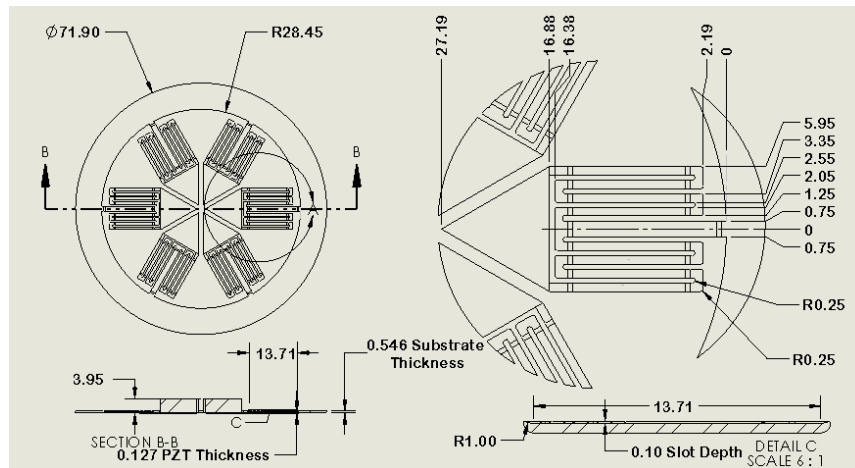
Figure 3.3: Detailed Drawing in mm Of PZT Substrate

26

Beyond its visual appeal, the design embodies an approach to versatility and flexibility. The energy harvesters in a circular arrangement are not merely an exercise in redundancy; they help to improve the harvester's reliability by fortifying the system against potential failures in one or more legs. This redundant architecture endows the overall structure with resilience, elevating the system's robustness. Each beam link in each leg is equipped with PZT-5H strips, each having a thickness of 127 μm for electricity generation. Finally, a tip mass is directly printed to the opposite end of each leg to ensure the harvester has a fundamental natural frequency well below the natural frequency threshold of 100 Hz.
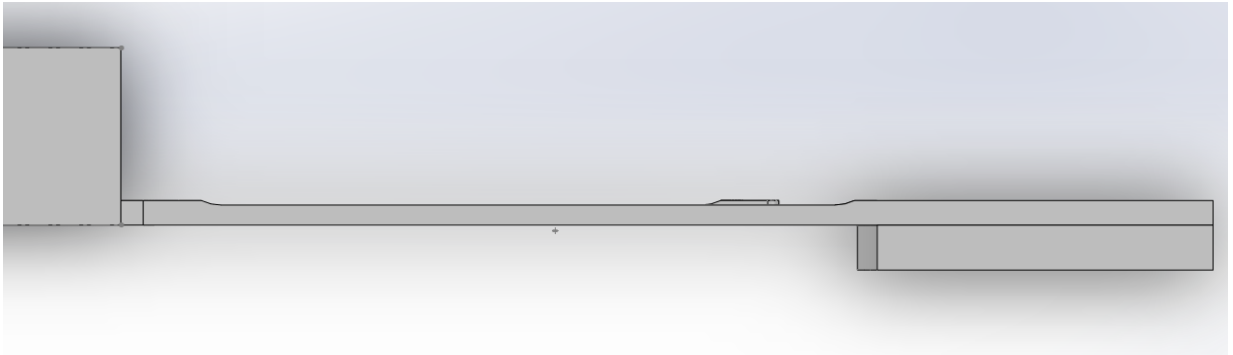
Figure 3.4: Cross-section view of the substrate to show the nonuniform shape of the beam.

This structure's fabrication process leverages metal additive manufacturing capabilities, allowing tremendous design freedom. In contrast to conventional methods, this fabrication approach enables a change in the thickness of each beam link within the harvester, as shown in figure 3.4. This design effectively lowers the fundamental natural frequency and optimizes the structure to sustain the necessary structural integrity to withstand high-stress conditions during operation.

3.3.2   Modelling and Simulation Setup

The 3D model was designed using SOLIDWORKS to create the virtual representation of the harvester, as shown in Figure 3.5. The subsequent step advanced into dynamic simulation, employing the COMSOL 6.0 Multiphysics Finite Element Analysis (FEA) software package. To optimize computational efficiency without compromising accuracy, the design's symmetrical attributes allow for simulating only one leg of the structure, as shown in Figure 3.6, expediting the retrieval of crucial insights, including the structure's strain distribution, natural frequency, and mode shape.
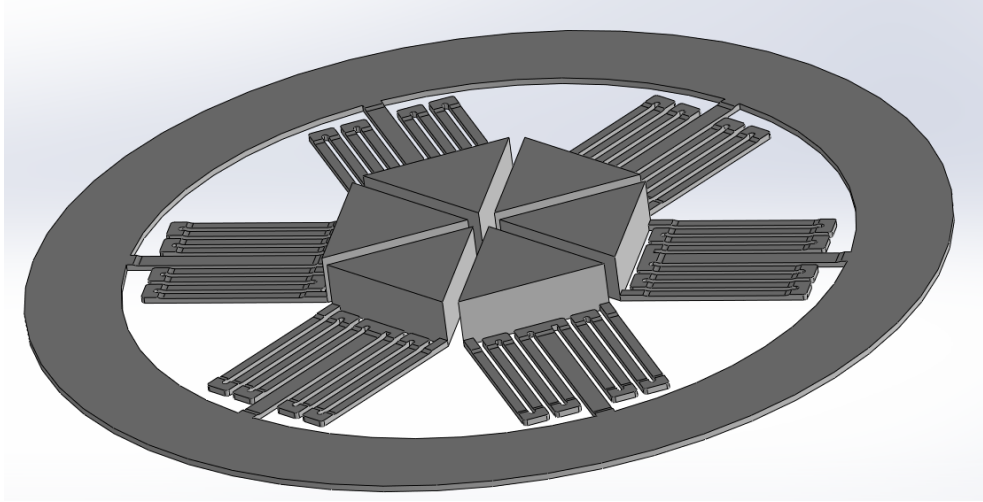
Figure 3.5: 3D model of the energy harvester in Solidworks.
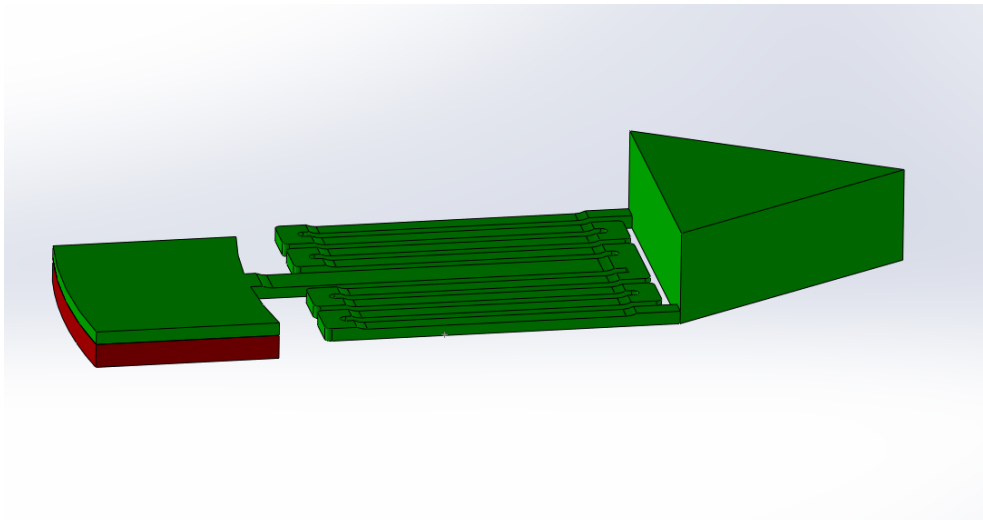
Figure 3.6: 3D simplified model of the energy harvester for FEA study in Solidworks.

An indispensable aspect of setting up the FEA model lies in the correct input of the mechanical properties of the substrate material. In this context, Matweb specifically provides details about the mechanical characteristics of the 17-4PH H900 condition as detailed in table 3.2 [37], help unveil attributes essential for comprehending its behaviour during simulation.

The pivotal piezoelectric material, PZT-5H, assumes a central role in the project, and its mechanical and electrical properties were deprived of the supplier's website [35]. figures 3.7, 3.8, and 3.9 present the data used for the simulation, such as the compliance matrix, the coupling coefficients matrix, and the relative permittivity matrix, respectively.

Table 3.2: Mechanical Properties of 17-4PH H900

Young's Modulus	197 GPa
Density	7800 kg/m^3
Poisson's ratio	0.272
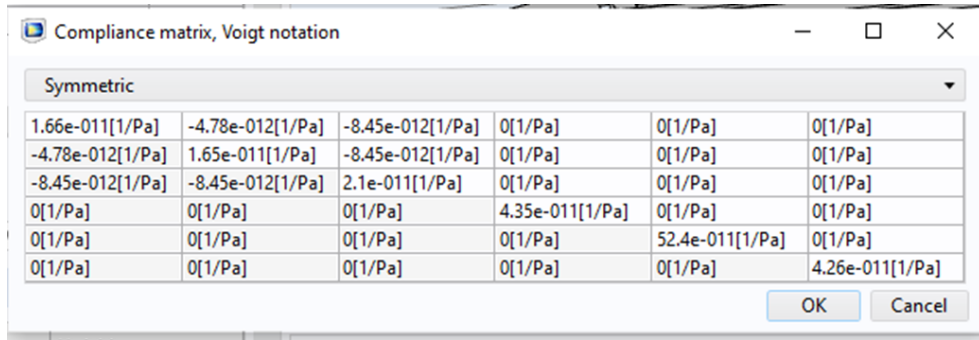
Figure 3.7: PZT-5H compliance matrix
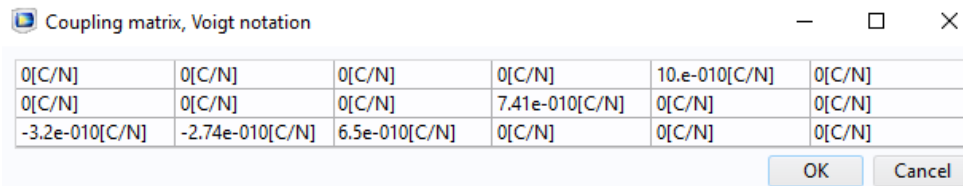
Figure 3.8: PZT-5H coupling matrix
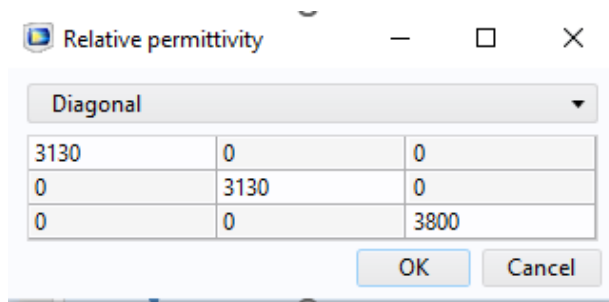
Figure 3.9: PZT-5H relative permittivity

Other critical aspects of FEA include defining boundary conditions and mesh generation. In this case, the boundary condition is established as fixed at the clamped end of a cantilever beam indicated as red in Figure 3.6, while the other end, with a tip mass directly printed onto the substrate, is left free.

After conducting numerous experiments and trials, it has been established that a "normal" mesh is the optimal choice for the application. This type of meshing produces accurate results and minimizes computational time with the optimal number of nodes that need to be solved. The meshing configuration for the model is visually represented in figure 3.10.

| MESH STATISTICS	
Description	**Value**
Status	Complete mesh
Mesh vertices	3753
Tetrahedra	12379
Triangles	6884
Edge elements	1828
Vertex elements	275
Number of elements	12379
Minimum element quality	0.06942
Average element quality	0.5445
Element volume ratio	2.2702E-8
Mesh volume	426.3 mm³

Figure 3.10: FEA meshing information in COMSOL

3.3.3 Simulation

3.3.3.1 Modeshape

The eigenanalysis was performed to obtain the fundamental natural frequency of the substrate with the PZT attached, accompanied by a virtual representation of the associated mode shape in figure 3.11. This analysis was conducted for two scenarios: one with uniform thickness and another with non-uniform thickness. The analysis reveals a significant reduction in the natural frequency from 79.507 Hz to 63.955 Hz when comparing the characteristics of model A (uniform thickness) to model B (non-uniform thickness). This achievement is remarkable, given the inherent challenges of reducing the natural frequency in a compact structure.

In addition, using the mass at the tip ends is incorporated as an additional strategy for reducing natural frequency. However, it is imperative to highlight that pursuing such an

approach comes with the trade-off of requiring a significantly increased amount of material to attain the desired natural frequency. Additionally, the increase in mass, which leads to an increase in force, adds more stress to the system, potentially resulting in the harvester failing during operation. Therefore, it is essential to accurately calculate and simulate the mass weight depending on the desired natural frequency.
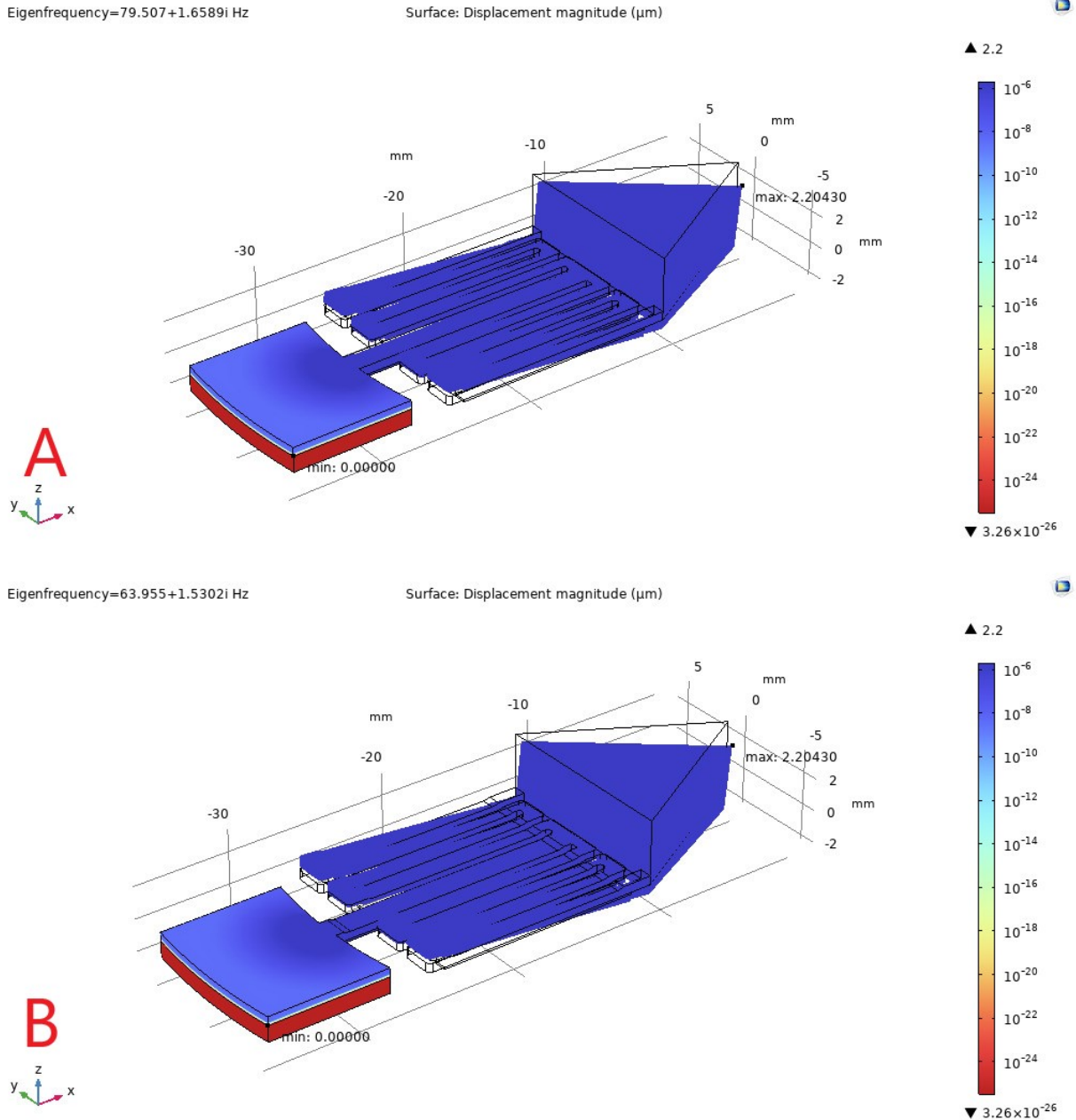
Figure 3.11: Energy Harvester modeshape and fundamental natural frequency. A is uniform thickness, and B is nonuniform thickness.

Furthermore, the model shows the profound advantages of adopting advanced 3D additive

manufacturing techniques over traditional methods for substrate fabrication, such as laser cutting. The ability to optimize the substrate geometry thickness allows a more freedom approach to structural design.

3.3.3.2 Strain Plot

During the eigenanalysis study, it became evident that the strain plot pattern, as visually represented in figure 3.12, exhibited a distinct and orderly alternation between tensile and compressive strains within each section of the symmetrical zigzag cantilever beam when subjected to cyclic loading. This particular strain distribution highlights a well-organized response to the mechanical stresses induced upon the structure.
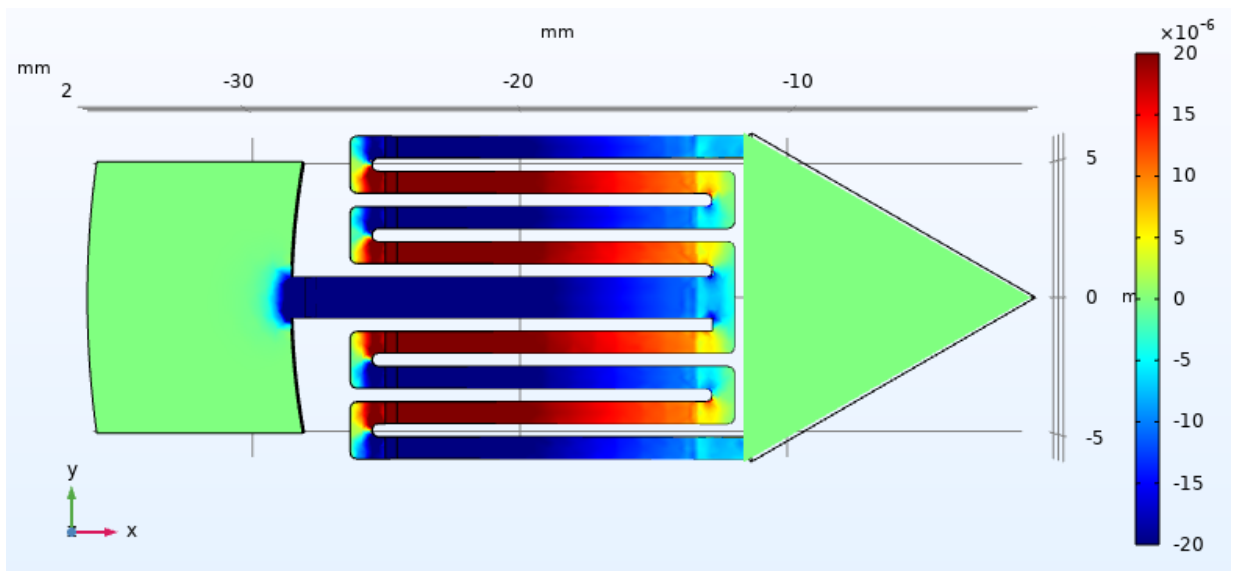
Figure 3.12: Strain plot of the substrate during first mode vibration

Moreover, the plot shows strain nodes at the connection point within the beam. This strain node introduces the potential for electrical cancellation due to the change in the sign of stress. However, the overall structure showcases a consistency characterized by a nearly pure bending behaviour. This behaviour is essential to energy harvesting, as it is ideal for efficiently converting mechanical energy into electrical power. This thesis excludes the strain plot study of higher-order natural frequencies. The rationale behind this decision lies in the tendency of such higher-order modes to generate a mode shape that leans towards torsional dominance. Harvesting energy in the higher modes would require the integration

of complex PZT pattern design and wiring strategies, which fall beyond the defined scope
of the research.

3.3.3.3 Loading Conditions

The solid mechanic's options employ the body load feature to apply cyclic loading. This
assumes a single input acceleration, oriented in the direction of gravity as described in
figure 3.13, and can be expressed as follows: "solid.rho*g_const*acc", where "solid.rho"
represents the object's mass in kilograms (kg), g stands for the gravitational constant in
meters per second squared (m/s^2), and acc is a variable fractional acceleration value. For
instance, if the acceleration input matches the gravitational constant, acc is set to 1 in the
parameter1 under the global definitions section, as shown in figure 3.14.
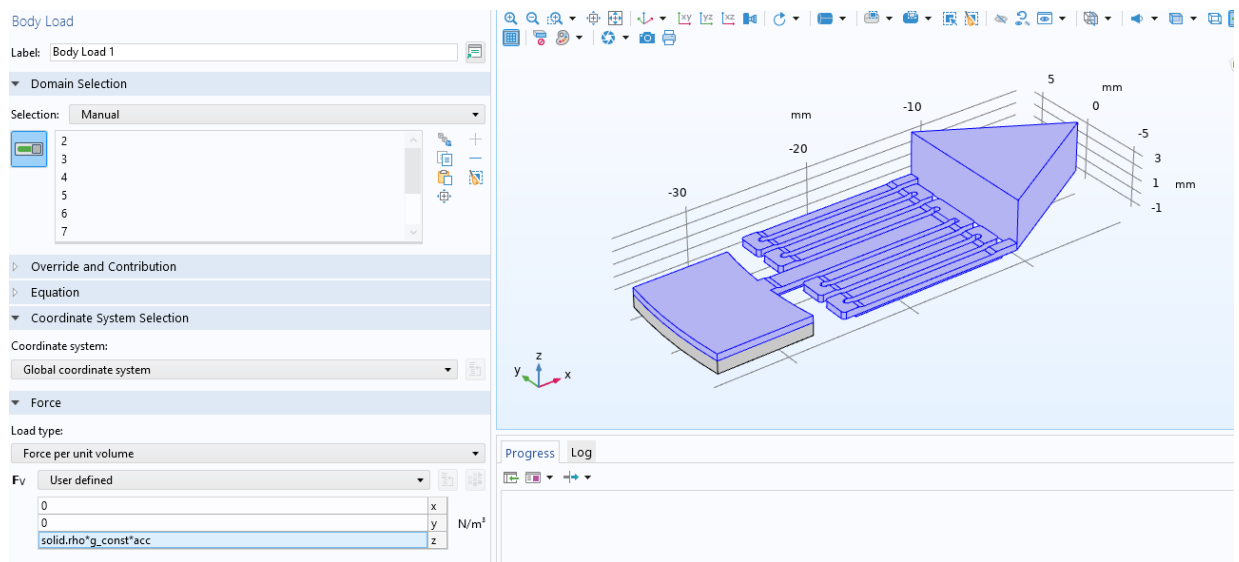
Figure 3.13: Input acceleration using Body load module in COMSOL
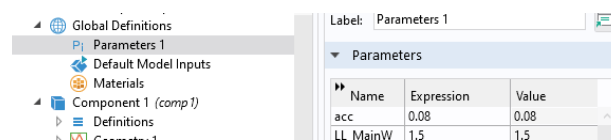
Figure 3.14: variable fractional acceleration value (acc)

3.3.3.4 Power And Voltage Simulation

The model has been specifically designed to replicate the Piezoelectric effect by quantifying
the RMS voltage and power output, subsequently making a comparative analysis with

33

experimental data. The mathematical expressions utilized in COMSOL to derive the RMS voltage and power output can be found in figure 3.15. Within this model, the variable R1 represents an external resistance, and it is incorporated into the system as a parallel connection with the PZT strips. Consequently, the RMS voltage across the entire circuit is computed by measuring the RMS voltage of R1.

Expression	Unit	Description
(abs(cir.R1_v)/(1.414))	V	Voltage
0.5*realdot(cir.R1_v,cir.R1_i)	W	Power

Figure 3.15: Power and voltage expressions in COMSOL

Furthermore, the power calculation aims to determine the maximum power output, which occurs when the internal resistance of the PZT material matches the external resistance R1, as detailed in [41]. An experimental resistance sweep was conducted in the lab to find the optimal resistance for maximum power. The voltage output was recorded for each external resistance value to calculate the power output. After identifying the optimal resistance, the power expression in figure 3.15 was modified with an intentional adjustment by adding '0.5' to the power expression during the resistance sweep to simulate the scenario where the internal resistance equals the external resistance, effectively halving the power value.

Chapter 4

Fabrication, Experimental Procedure, Result and Validation

4.1 Fabrication

This section offers an extensive examination of the complete fabrication process for the PZT energy harvester, encompassing various advanced fabrication techniques used in this project from inception to conclusion; the fabrication process flow is described in Figure 4.1.

Figure 4.1: Energy Harvester Fabrication Process Flowchart

4.1.1 Additive Manufacturing

The proposed substrate design is characterized by a nonuniform thickness, presenting challenges for traditional manufacturing processes, especially at the micro level. In response to this limitation, 3D additive manufacturing techniques are employed. The manufacturing method allows for creating complex design details that would be otherwise difficult to achieve using conventional techniques. By leveraging the capabilities of 3D additive manufacturing, the goal is to overcome the constraints imposed by the nonuniform thickness

of the substrate. This strategic choice addresses inherent challenges in the manufacturing process and opens up new possibilities for achieving innovative and customized substrate structures.

Figure 4.2: Renishaw AM400 pulsed laser PBF machine

The Multi-Scale Additive Manufacturing Lab managed the substrate fabrication at the University of Waterloo. The 17-4 stainless steel substrate metal powder was prepared and printed on a metallic plate using the Renishaw AM400 laser powder bed fusion machine at its original setting, as shown in Figure 4.2 [42]. After finishing printing the substrate, the metallic plate was removed from the machine with the printed substrate on top, as presented in Figure 4.3
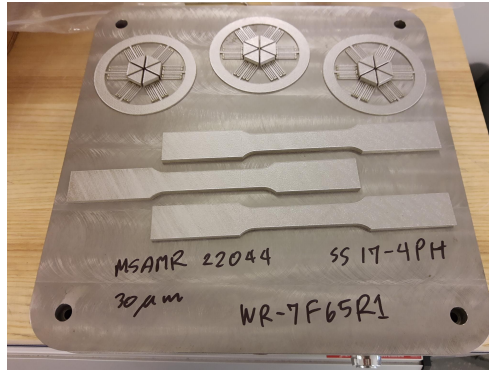
Figure 4.3: Finished Printed Substrate

The last phase of the processing is to separate the substrate from the base plate. A wire electrical discharge machine, as shown in Figure 4.4 [43], was employed to ensure the smooth removal of the substrate while preserving its thickness dimensions. Figure 4.5 shows the substrate after removal.

Figure 4.4: Sodick VL600QH Wire Electrical Discharge Machining (EDM) System
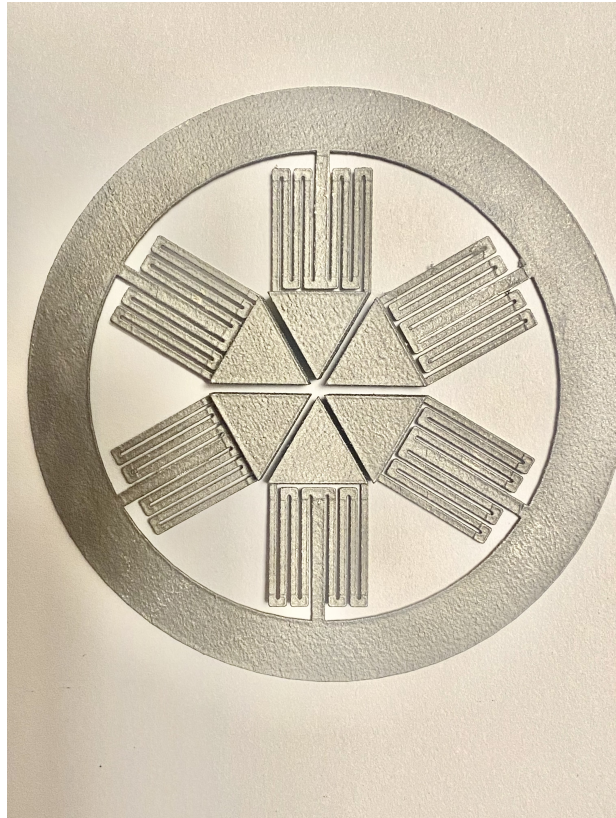
Figure 4.5: substrate after removing from the EMD machine

4.1.2 Heat Treatment Process

After removing the substrates from the base plate, a critical step in enhancing their mechanical characteristics was undertaken through heat treatment. Specifically, this process is identified as age-hardening, a well-established technique applicable to 17-4PH stainless steel. The intricacies of this age-hardening process involve subjecting the 17-4 stainless steel components to a carefully calibrated heat treatment within an oven, as illustrated in Figure 4.6, precisely at a temperature of 1038°C for one hour [44]. This initial stage is known as the solution heat treatment or A-condition. In the AMS5355 standard, the homogenization heat treatment was carried out before the solution heat treatment; however, due to the temperature limit of the oven, the homogenization was skipped because the required yield strength can also be achieved with solution treatment followed by age-hardening heat treatment [38].

Figure 4.6: Knol oven from Surface Science and Bio-nanomaterials Lab at University of Waterloo

Following the solution heat treatment, the substrate was cooled at room temperature before being reintroduced into the oven. This second phase of heat treatment involved exposing the substrate to a temperature of 483°C for an additional duration of 1 hour and 30 minutes, resulting in what is termed the H900 condition [44]. Figure 4.7 visually represents the substrate post-heat treatment.

The H900 condition achieved through this heat treatment process is noteworthy for its significantly heightened yield strength while concurrently preserving the Young Modulus

of the substrate compared to its 3D-printed counterpart. This enhancement in mechanical properties is paramount in applications where superior strength characteristics are imperative. A comprehensive summary of the yield strength and ultimate tensile strength (UTS) values for both the 17-4PH as-built and H900 conditions can be found in Table 4.1, with data sourced from [38].

Table 4.1: 17-4PH Yield Strength and UTS in MPa at as-built and H900 conditions

	As-built	H900
Yield Strength	860.6	1170.0
UTS	886.0	1310.0
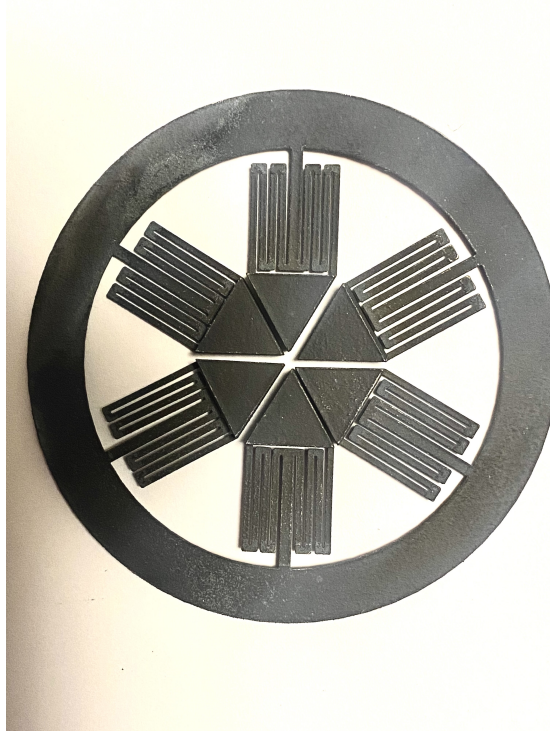
Figure 4.7: The substrate after heat treatment

4.1.3   PZT Material Fabrication Process

The objective of PZT fabrication is to create basic rectangular shapes; however, the process of fabricating PZT-5H posed a substantial challenge due to the thinness of the material (127µm) and its inherent fragility of the PZT's material. Therefore, due to the micro-scale

dimensions of this delicate material, its fabrication process requires a highly specialized approach.
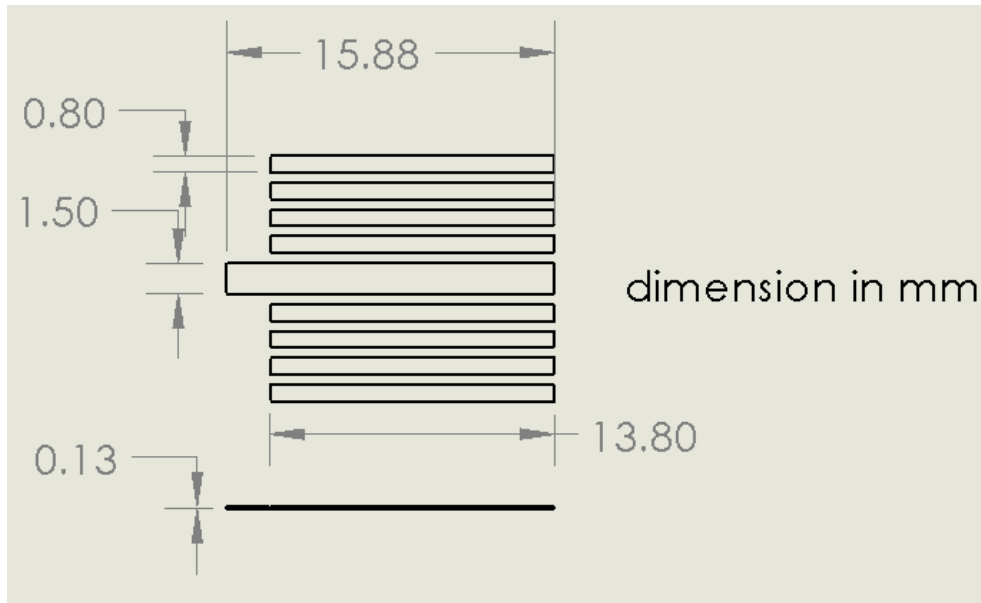
Figure 4.8: PZT strips pattern on the substrate

To address the issue, Kadco Ceramics provided a machining service to machine the PZT-5H (Navy Type VI) ceramics sheet, sourced from PIEZO.com, into various rectangular configurations encompassing two distinct sizes, as described in Figure 4.8. The dicing method was used to cut the PZT sheet into smaller pieces precisely, which offers a significant advantage as it can maintain high precision dimensions while generating minimal heat due to the constant coolant circulation and the brief contact between the workpiece and the cutting tool.

Before dicing processing, the PZT sheet was prepared by wax-mounting it onto a piece of glass. This preparatory step is crucial to safeguard the fragile material during fabrication and transportation. The final products of this intricate fabrication process are shown in Figure 4.9 and 4.10.
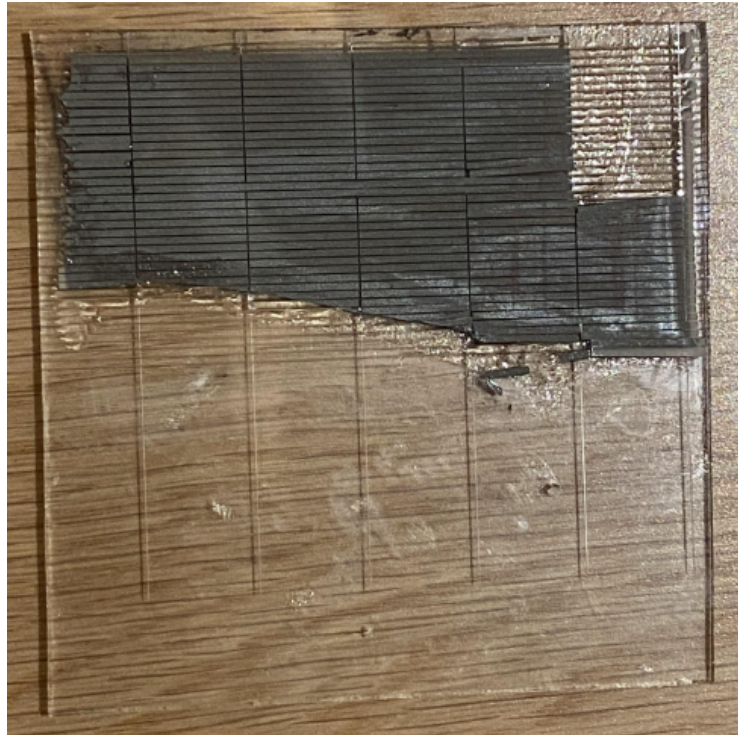
Figure 4.9: PZT small strips after dicing
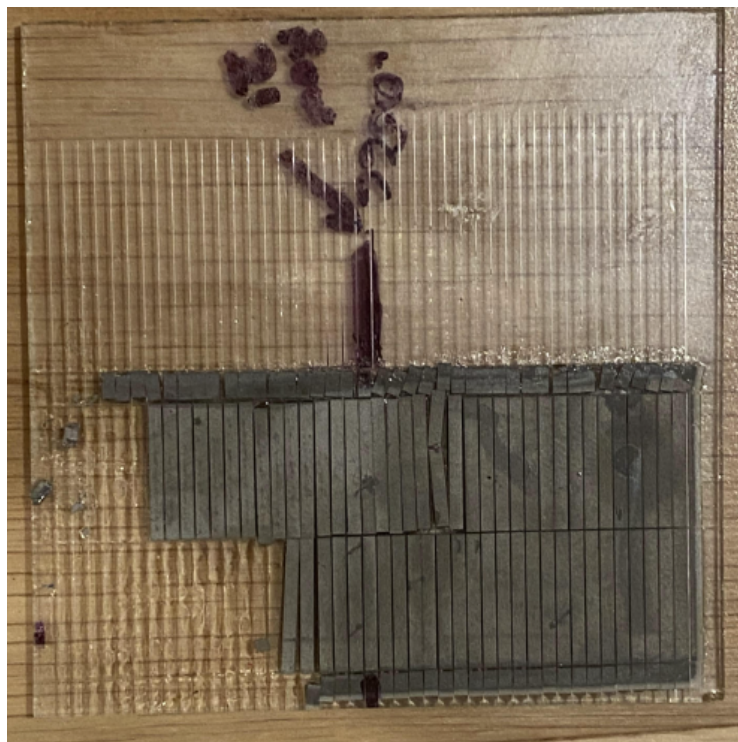
Figure 4.10: PZT wide strips after dicing

4.1.4 Energy Harvester Fabrication Process

This section presents the process of affixing PZT strips to the substrate. To remove PZT strips from the glass as shown in Figure 4.9, 4.10, the glass was subjected to a temperature of 90°C to melt the wax, which allowed the removal of the PZT strips from the glass. Subsequently, PZT strips were bathed in Acetone to eliminate any residual wax on the surfaces of the PZT strips. Before attaching these strips to the structural beams, it was imperative to determine their arrangement accurately, as each beam experiences distinct strains, either positive or negative. Each beam within the framework is individually linked to a dedicated PZT strip to avoid charge cancellation that arises from a continuous PZT structure [45]. Additionally, to streamline the wiring procedure, a conductive silver epoxy adhesive is utilized to fasten the PZT strip to the structure, concurrently serving as a ground connection. The polarization of the PZT strip is aligned with the local strain to ensure compatibility with the strain; the technique is known as strain-matched polarization (SMP) [45].

The AA-DUCT 907 Silver Conductive Epoxy manufactured by Atoms was used by mixing the resin and hardener in a 1:1 ratio. This mixture was applied to one side of the PZT strip before being precisely positioned on the substrate using tweezers. This procedure was repeated for all the beams on the substrate. The subsequent stage involves curing the energy harvester to allow the epoxy to firm up. The process can be achieved by either allowing it to cure at room temperature for 24 hours or placing it in a heat chamber at 50°C for 45 minutes. Aceton was used after curing to clean the energy harvester to remove excessive epoxy and prevent potential short circuits. The outcome is illustrated in Figure 4.11.

Figure 4.11: PZT Energy Harvester

4.2 Experimental Procedure, Result and Model Validation

The experimental procedure is described in this section, with the primary objective of validating the Finite Element Analysis (FEA) model. The experiment aims to verify and fine-tune the system parameters, ensure a precise alignment between the physical model and the simulated results of the PZT energy harvester, and construct frequency response plots encompassing displacement and voltage parameters. It involves subjecting the physical model to a range of frequencies to capture its response in terms of both displacement and voltage output. The comprehensive frequency response plot generated through this experiment serves as a crucial benchmark for validating the simulated results against real-world observations.

Moreover, this experiment aims to optimize the external resistance load applied to the PZT energy harvester. By systematically varying the external load, the objective is to identify the optimal conditions that maximize the output power generated by the harvester. This optimization process is vital for harnessing the full potential of the energy harvesting system, ensuring that it operates at peak efficiency under real-world conditions.

4.2.1 General Setup

The experimental configuration involves situating the entire energy harvester on the test bench, as illustrated in Figure 4.12. An electromagnetic shaker is employed to induce excitation in the PZT energy harvester, utilizing a base excitation mechanism with a precisely controlled 0.08g acceleration input. The Modal Shop's versatile 2075E shaker, securely fastened to the ground using industrial clamp straps and oriented vertically, is chosen for this purpose. This shaker model is precisely engineered to deliver an output force of 334 N, encompassing a broad frequency range of up to 6500 Hz [46].
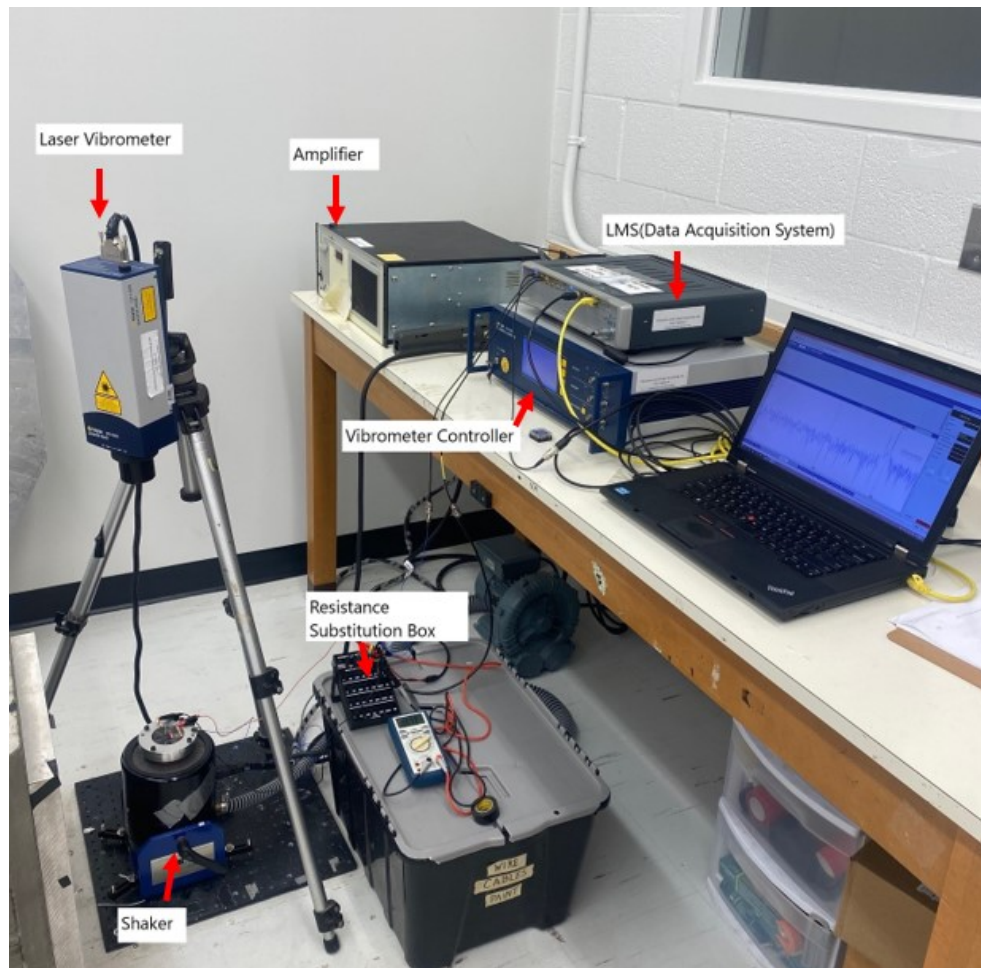
Figure 4.12: PZT energy harvester experimental test setup

The PZT energy harvester is affixed to the shaker using a dedicated fixture, as shown in Figure 4.13. This fixture was designed to ensure a secure and precise mounting of the energy harvester on the shaker, facilitating the controlled application of mechanical vibrations during the experimental procedure.
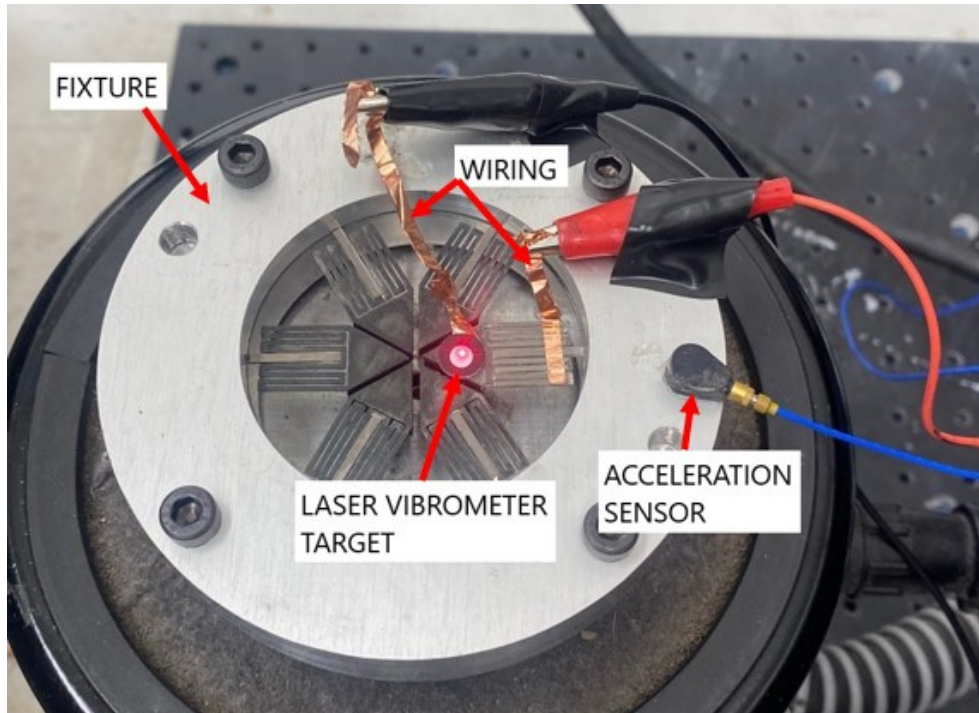
Figure 4.13: PZT energy harvester test fixture and wiring setup

The experimental control system employed the Siemens LMS SCADAS Mobile data acqui-
sition system, which implemented a closed-loop control model for precise command and
feedback operations. The LMS software then communicated commands to the LMS system
through an Ethernet connection. The LMS system, acting as the center, is interfaced with
multiple input-conFigured ports to measure and record data in real-time from various pa-
rameters such as displacement, acceleration, voltage, current, and more. In addition, the
LMS system has 2 output ports that can be conFigured to feed various signal types (sine,
burst, etc..), which are fed into a linear power amplifier (Modal Shop Model 2050E09) in
order to drive the shaker.

A PCB model 352A24 accelerometer, which has a sensitivity level of 100.9 mV/g and
an operational frequency range of up to 10,000 Hz [47], was utilized to gauge the actual
acceleration induced by the shaker. The closed-loop feedback mechanism, controlled by
the LMS software, aimed to dynamically adjust the shaker's acceleration output to match
the commanded input from the computer, ensuring precise control during the experiment.

A Polytec model OFV505 laser vibrometer, coupled with the Polytec control unit model
OFV5000, was employed to monitor the displacement of the energy harvester. This laser
vibrometer directed a beam onto a target affixed to the PZT energy harvester, capturing

displacement data based on the Doppler effect principles [5]. The acquired data underwent Fast Fourier Transform signal processing, which was processed by the LMS software to produce the Frequency Response Function (FRF) plot for displacement.

Simultaneously, electrical signals generated by the PZT were captured using crocodile clamps and transmitted to the LMS system. This process enabled the generation of the FRF plot for Root Mean Square (RMS) voltage, providing insights into the energy harvester's electrical performance.

An Elenco resistor substitution box was incorporated to optimize the external resistive load applied to the PZT energy harvester. This device allowed a resistance sweep, allowing for the identification of the optimal external resistive load that maximizes the harvester's output power. Integrating these advanced measurement and control components forms a robust experimental setup for comprehensive analysis and optimization of the PZT energy harvester under various operating conditions.

4.2.2 Experimental and Simulation Results

4.2.2.1 Experimental and Simulation Displacement Comparison and Damping

This section presents the outcomes of the energy harvester testing, where the unit underwent base excitation at 0.08g acceleration. The experiment involved a frequency sweep to acquire the displacement Frequency Response Function (FRF) plot. During this testing phase, the laser vibrometer accurately captured the displacement of the energy harvester by projecting the laser onto the harvester around the centroid of the triangle tip mass.

This methodical frequency sweep allowed for a detailed exploration of the energy harvester's response across different frequencies, providing a comprehensive understanding of its dynamic behaviour. The FRF plot, produced from this testing, serves as a crucial visual representation of how the harvester responds to varying levels of base excitation, shedding light on its resonance characteristics and performance.
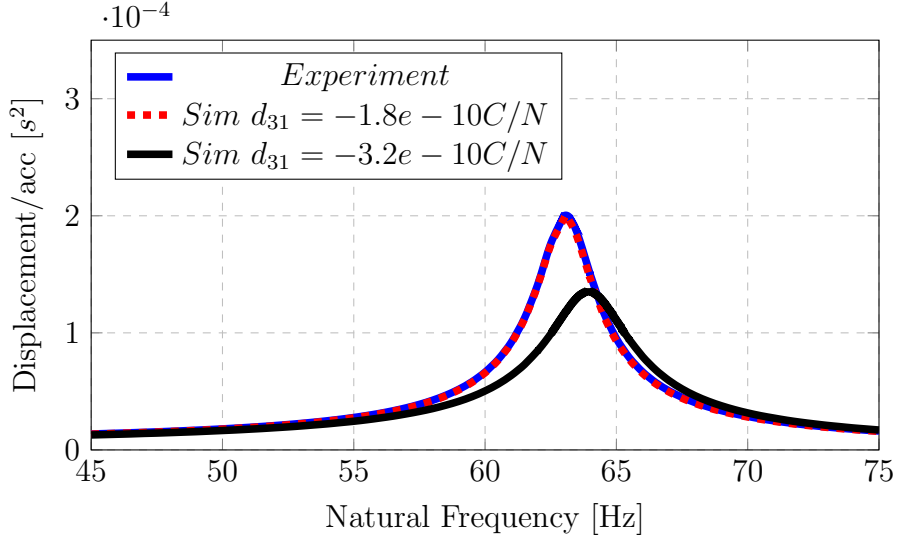
Figure 4.14: Displacement FRF of the energy harvester

Due to the researchers' focus on harvesting energy from the primary bending mode of vibration, a shaker test was conducted to precisely capture the energy harvester's displacement at its fundamental natural frequency. This involved subjecting the structure to a sweep frequency range of 45 to 75 Hz. The results of this physical experiment are displayed graphically in Figure 4.14, supplemented by computer simulations replicating the same frequency range. During the experiment, the first bending mode was identified at 63.05 Hz. However, this outcome in terms of displacement plot and natural frequency differed from the prediction made by the simulation model, which anticipated the first bending frequency at 63.96 Hz with $d_{31} = -3.2 \times 10^{-10}$C/N—remarkably, adjusting the simulation model with $d_{31} = -1.8 \times 10^{-10}$C/N brought about substantial agreement in the displacement FRF plot concerning the first fundamental natural frequency (63.05 Hz vs. 63.065 Hz) and the peak amplitude.

The observed reduction in the coupling coefficient between the simulation parameter and the vendor-supplied data suggests potential internal fractures within the PZT strips introduced during the fabrication process. The fracture led to a decrease in stiffness, resulting in heightened displacement. Moreover, the PZT strips were exposed to external heat for their removal from the glass by melting the wax used to hold them in place. In an agreement with this idea, Suaprasert *et al.* [48] demonstrated that d_{31} for PZT-5H material tends to decrease after exposure to temperatures surpassing 100°C due to internal fractures. The current paper lacks information regarding the extent of fracture within the harvester; thus,

potential degradation could commence at temperatures below 100°C.

Employing the quadrature peak picking method [49], the damping ratio was extracted from the experimental data, and subsequently, the loss factor was computed using Equation 4.1 [50], optimized to approximately 0.271 to align with the displacement peak of both simulation and experiment. This optimized value was then used to update the damping section of the Linear Elastic Material module and the mechanical damping module within the PZT section in the Comsol model, as illustrated in Figure 4.15.

$$\eta = \frac{1}{Q} = 2\zeta$$

$$Where:$$

$$\eta \ loss \ factor$$ \hfill (4.1)

$$Q \ quality \ factor$$

$$\zeta \ damping \ ratio$$
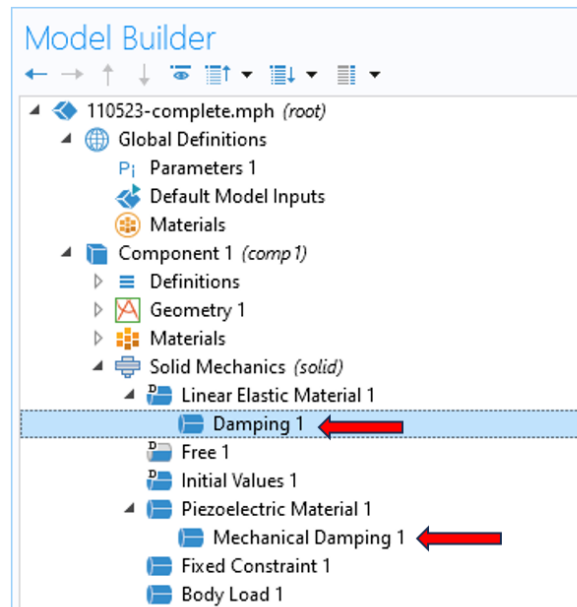
Figure 4.15: Comsol Simulation Damping Module

4.2.2.2 Experimental Optimal External Load Resistance

A resistance sweep was conducted to identify the optimal resistance for the energy harvester in order to produce the highest power. The experimental setup involved utilizing an external resistance box, connecting in parallel with the energy harvester. The maximum power was determined by applying Equation 4.2 to the recorded voltage at each specific resistance setting.

$$P = \frac{V^2}{2R}$$

$$Where:$$

$$P \ power \ [W]$$

$$V \ maximum \ voltage \ [V]$$

$$R \ resistance \ value \ of \ the \ external \ resistor \ [\Omega]$$

(4.2)

As explained by Ibrahim [41]; optimal power is achieved when the internal resistance in the PZT equals the external resistance from the substitution box. As a result, the resistance sweep involved changing the resistance box and continuously recording the power. The outcomes of this resistance sweep are documented in Table 4.2.

Figure 4.16 presents a graphic representation of the resistance sweep results. As observed, the optimal power of the energy harvester was identified at 200,000 Ω. This crucial information was subsequently utilized to update the resistance value employed in the simulation model, ensuring that the simulated conditions align closely with the experimentally determined optimal resistance.

Table 4.2: Resistance value with its power

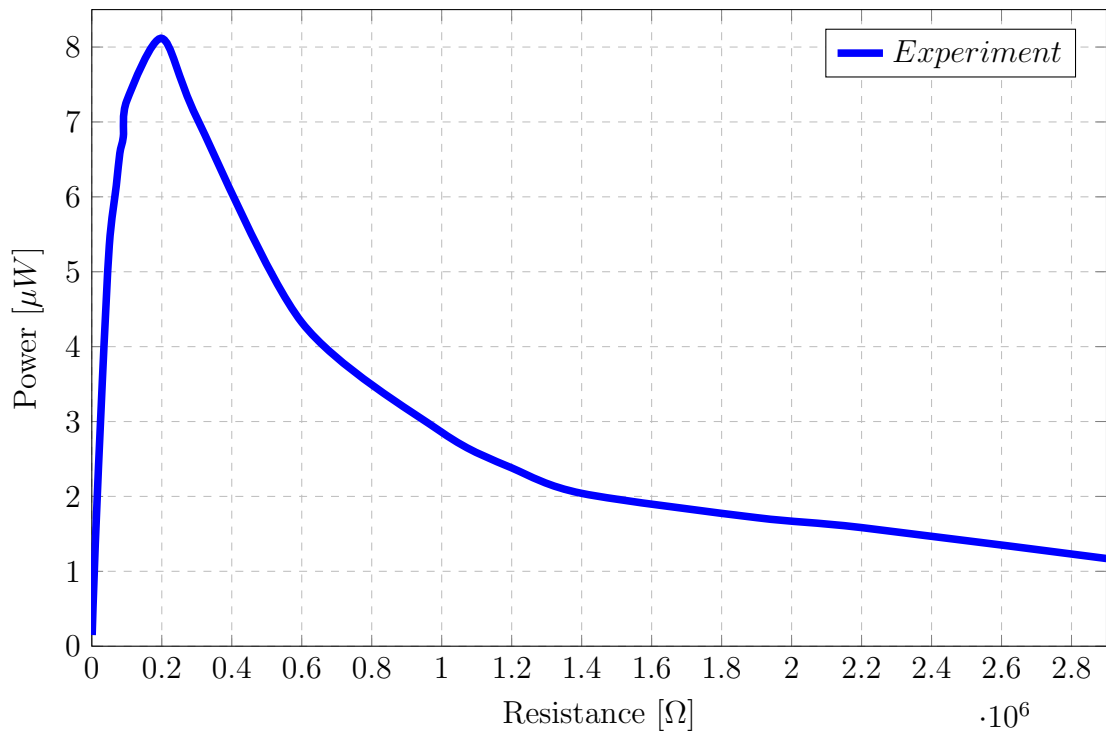| Resistance [Ω]	voltage [V]	power [μW]
1000	0.017	0.149
10000	0.165	1.367
30000	0.460	3.531
50000	0.731	5.347
70000	0.928	6.154
80000	1.026	6.584
90000	1.107	6.803
100000	1.207	7.283
200000	1.802	8.116
300000	2.057	7.055
600000	2.278	4.324
1000000	2.391	2.857
1200000	2.391	2.381
1400000	2.391	2.041
1900000	2.554	1.716
2200000	2.640	1.584
2900000	2.606	1.171

Figure 4.16: Resistance optimization plot

4.2.2.3 Experimental and Simulation Voltage Comparison

In the preceding section, the examination focused on a comparative analysis involving the simulation model and experimental data, particularly emphasizing the coupling coefficient and displacement FRF plot. When comparing the voltage output obtained during the experiment as shown in Figure 4.17, with d_{31} set at -1.8 $\times 10^{-10}, C/N$, the simulation model is well aligned with the experimental data for the Root mean square (RMS) voltage FRF, displaying a corresponding peak in both amplitude and natural frequency (63.05 Hz).

On the other hand, when employing the d_{31} of -3.2 $\times 10^{-10} C/N$ as provided by the vendor's data sheet [35], the model indicates an increase in voltage coupled with a shift in natural frequency—approximately 64 Hz, deviating from the experimental data's 63.05 Hz. This outcome substantiates the assertion that the actual coupling coefficient in the PZT material is lower than the vendor's advertised value. This comparison aims to compare these outcomes with the experimental data and the simulation model characterized by d_{31} = -1.8 $\times 10^{-10} C/N$. This comparative analysis sheds light on the impact of temperature variations on the coupling coefficient, thus enhancing the understanding of the material's response under diverse operating temperature conditions.
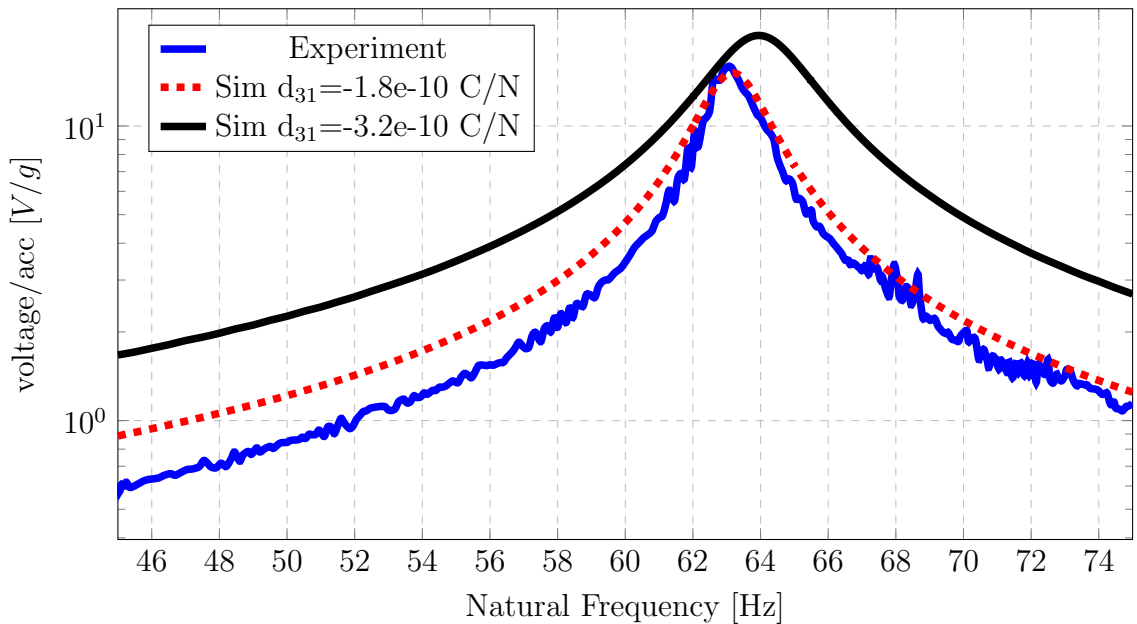
Figure 4.17: voltage FRF of a singular leg of the energy harvester

4.2.2.4 Power Calculation and Comparison To Other Works

In this section, the power computation for each model involves integrating the area under the power FRF curve. The power value is determined by using the Equation 4.3. The RMS voltage obtained from the experiment was converted to voltage data by multiplying with $\sqrt{2}$ to obtain the data for the power FRF plot. The input power bandwidth considered for power calculation is confined within the range defined at 2 different natural frequencies with the same power value, which is derived from the maximum RMS voltage, as illustrated in Figures 4.18 to 4.20. In addition, the resistance value employed in the computation is held constant at 200,000 Ω, a value identified from the experiment detailed in the previous section. Table 4.3 presents the resultant power range values and total power.

$$\text{power}(W) = \frac{\text{power Area under the peak (W} \cdot \text{Hz)}}{\text{Bandwidth (Hz)}} \tag{4.3}$$

Figure 4.18: Experimental power FRF of the Energy Havester

Figure 4.19: Simulation power FRF @ $d_{31} = $ -1.8 $\times 10^{-10}$ C/N of the Energy Havester
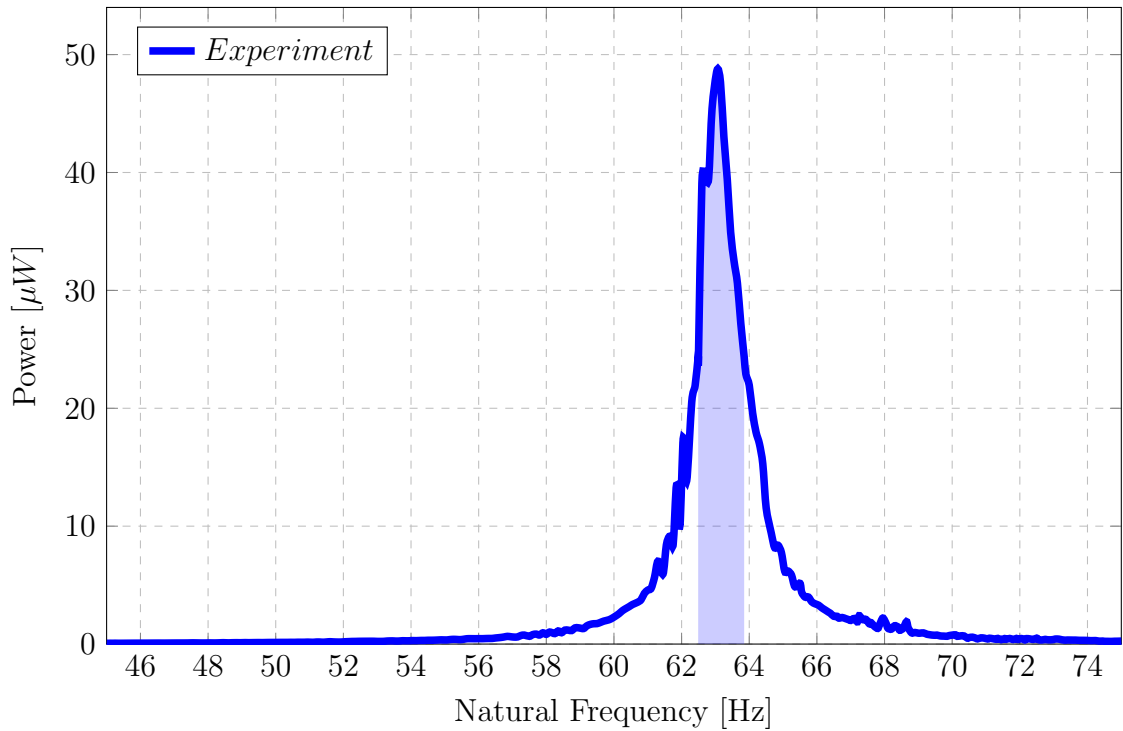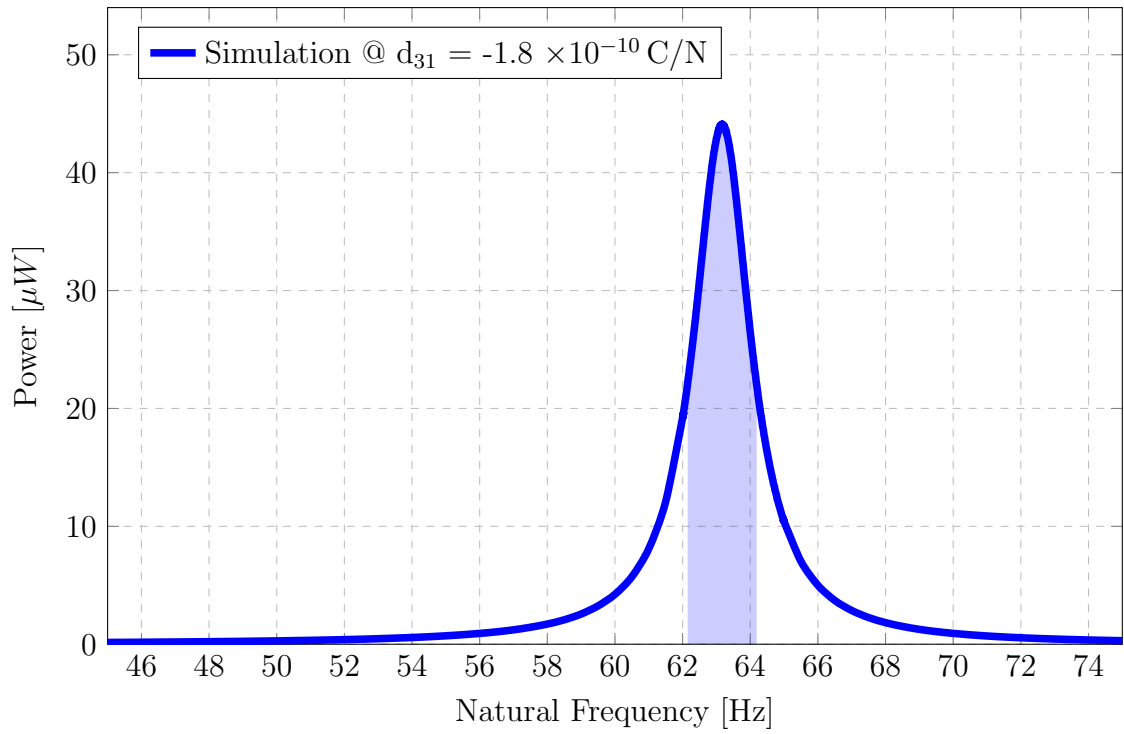

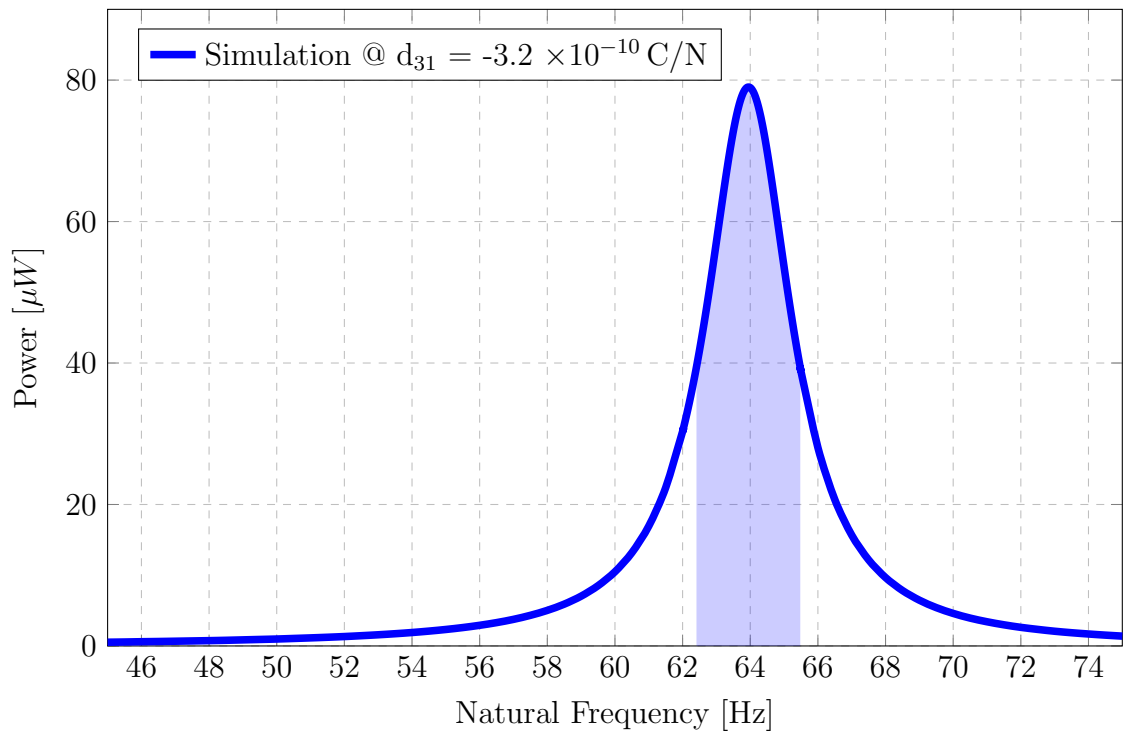Figure 4.20: Simulation power FRF @ $d_{31} = $ -3.2 $\times 10^{-10}$ C/N of the Energy Havester

Table 4.3: Maximum power and RMS voltage power

Model Type	Maximum power [μW]	RMS voltage power [μW]	Total power Under The Curve [μW]
Experiment	48.70	24.35	39.27
Simulation @ d_{31} = -1.8 $\times 10^{-10}$ C/N	44.06	22.16	34.80
Simulation @ d_{31} = -3.2 $\times 10^{-10}$ C/N	79.02	39.44	62.19

The power calculation results are presented alongside other designs sourced from Bath [2] in Table 4.4. Subsequently, a comparative analysis is undertaken to assess how the experimental and simulation results compared to other research on energy harvesters.

The normalized power density (NPD) is adopted as a normalized measurement standard to standardize the comparison metric across various research studies. This metric considers the device volume, excitation frequencies, and stimulating accelerations, as recommended by Liang *et al.* [51]. The calculation of NPD is performed following Equation 4.4, offering a consistent basis for evaluating and comparing the energy harvester models. This approach ensures a fair and meaningful comparison, considering the influence of different parameters and designs on the overall power density of the energy harvesting systems.

$$\text{NPD} = \frac{P}{A^2 V}$$

Where :

NPD *normalized power density* [kgsm^{-3}]

P power [μW]

A acceleration [ms^{-2}]

V volume [cm^3]

(4.4)

Table 4.4: NPD comparison between previous PZT energy harvesting technologies

Energy Harvester	Freq. [Hz]	Accel. [ms^{-2}]	Volume [cm^3]	power [μW]	NPD [kgsm^{-3}]
Experimental current design	63.05	0.78	1.864	39.27	34.63
Simulation @ d$_{31}$ = -1.8 $\times 10^{-10}$ C/N current design	63.17	0.78	1.864	34.80	30.69
Simulation @ d$_{31}$ = -3.2 $\times 10^{-10}$ C/N current design	63.95	0.78	1.864	62.19	54.84
Folded Zigzag [2]	95.6	9.81	2.12	18,800	92.00
Planar symmetric zigzag same tip mass per layer [2]	166.1	9.81	0.996	5800	60.51
Planar symmetric zigzag with the same natural frequency, extended leg [2]	95.6	9.81	1.424	9580	69.90
Karami [24]	8	1.18	8.6	110	9.19
Ibrahim *et al.* [41]	15 − 27	2.94	4.74	22	0.54
Beeby *et al.* [52]	52	0.589	0.15	46	884.0
Roundy *et al.* [53]	120	25	1	375	60.00

The analysis, observed from Table 4.4 [2], reveals that the current design surpasses Karami's and Ibrahim's designs regarding normalized power density (NPD). Even when compared to notable designs such as Folded ZigZag [45], Planar symmetric [45], and Roundy's design [53], which the current design exhibits lower NPD value, it showcases a promising prospect due to its lower natural frequency. This characteristic positions it favourably for substantial energy generation in low-frequency environments.

When comparing to Beeby *et al.*'s design [52], Beeby *et al.*'s design exhibits superior NPD compared to the current design and others in the literature; however, it is essential to know that only the volume of the magnet instead of the entire energy harvester unit was considered for NPD calculation of Beeby *et al.*'s design, resulting in an outlier NPD value as explained by Bath *et al.* [2]. Therefore, with its NPD value, the current design offers a sound choice for energy harvesting applications due to its power output and low natural frequencies.

The current design showcases promising performance in NPD, particularly excelling in low-frequency environments. Its favourable characteristics position it competitively among other energy harvester designs, offering a robust solution for scenarios where low-frequency vibrations are prevalent.

Chapter 5

Conclusion

5.1   Summary

Due to growing demands for clean energy to aim towards a net zero economy, researchers are looking into alternative energy sources to replace traditional lithium battery usage to power small electronic devices. One area of research is to replace the batteries for the WSN in remote areas, where it is impractical to physically replace them due to the high cost and causing environmental pollution at the end of battery life. This paper presents an innovative design inspired by the Vesper microphone arrangement concept [40] using elephant structure [26] to scale power output by placing multiple energy harvesters in a rim structure. In addition, additive manufacturing offered shorter fabrication time and allowed a much more complex design to lower the natural frequency. As a result, the design shows great potential in comparison with other researchers by having better NPD (34.63) than Karami (9.19) and Ibrahim (0.54) while offering a relatively low frequency (63.05 Hz) compared to Bath's design (95.6 Hz), Roundy et al's design (120 Hz) and Planar symmetric zigzag design (166.1 Hz with no extended leg and 95.6 Hz with extended leg). Furthermore, the power scalable capability of multi-energy harvesters on the structure provides great flexibility compared to other designs because it can operate partially if one or some units stop working.

5.2 Future Work

During the experiment, the PZT-5H strips used for the energy harvester exhibited a lower coupling coefficient (d31 = -1.8 $\times 10^{-10}$ C/N) in comparison to the value (d31 = -3.2 $\times 10^{-10}$ C/N) advertised by the supplier because of thermal exposure during the fabrication process. As shown in table 4.4, if the PZT possessed a similar value per the supplier, the NPD for the design could have been at 54.84, which is 58.36% higher than the actual design. Therefore, to address the issue, using different PZT materials for the design, which are less sensitive to thermal change during fabrication, will improve the mechanical-to-electrical conversion rate, resulting in higher power output.

In addition, introducing stress relief to eliminate residual stress after additive manufacturing can improve the substrate's fabrication process. Due to thermal expansion caused by additive manufacturing, the residual stress in the substrate distorted the substrate after the wire EDM machine removed it from the metal base. The behaviour results in uneven thickness between energy harvester units, causing fundamental natural frequency inconsistency. The distortion also posed a challenge when gluing the PZT to the substrate due to the uneven surface. Hence, stress relief before removing the substrate from the base can significantly improve the substrate geometry integrity and the adhesiveness of the PZT gluing process.

The wire bonding technique can be explored to improve the electrical circuit connection between PZT strips. Because of the size of the wiring (17.5 µm to 50 µm in diameter [54]), it helps reduce the damping and lower the stiffness of the overall structure, potentially leading to a further reduction in fundamental natural frequency.

Finally, further testing will need to be conducted to establish the operating conditions, such as the effective frequency span, maximum load, and fatigue testing, to ensure the sustainability of the energy harvester.

References

[1] Akyildiz I, WY S, Sankarasubramaniam Y, and Cayirci E. Wireless sensor networks: A survey. *Computer Networks*, 38:393–422, 03 2002.

[2] Bath D and Salehian A. A novel 3d folded zigzag piezoelectric energy harvester; modeling and experiments. *Smart Materials and Structures*, 28(2):025011, 12 2018.

[3] Noel A B, Abdaoui A, Elfouly T, Ahmed M H, Badawy A, and Shehata M S. Structural health monitoring using wireless sensor networks: A comprehensive survey. *IEEE Communications Surveys & Tutorials*, 19(3):1403–1423, 2017.

[4] Speirs J and Contestabile M. *The Future of Lithium Availability for Electric Vehicle Batteries*, pages 35–57. Elsevier, 02 2018.

[5] Fernandes E. Design, modelling, and fabrication of a low frequency piezoelectromagnetic energy harvester. Master's thesis, University of Waterloo, 2017.

[6] Alavi A H, Hasni H, Lajnef N, Chatti K, and Faridazar F. An intelligent structural damage detection approach based on self-powered wireless sensor data. *Automation in Construction*, 62:24–44, 2016.

[7] Erturk A and Inman D J. *Introduction to Piezoelectric Energy Harvesting*, chapter 1, pages 1–18. John Wiley I& Sons, Ltd, 2011.

[8] IER. Environmental impacts of lithium-ion batteries, May 2023. Accessed: 27 November 2023.

[9] Reilly E, Miller L, Fain R, and Wright P. A study of ambient vibrations for piezoelectric energy conversion. *Proc. PowerMEMS*, 01 2009.

[10] Sezer N and Koç M. A comprehensive review on the state-of-the-art of piezoelectric energy harvesting. *Nano Energy*, 80:105567, 2021.

[11] Leo D J. *Piezoelectric Materials*, chapter 4, pages 122–204. John Wiley & Sons Ltd, 2007.

[12] Lu X and Proulx T L. Single crystals vs. pzt ceramics for medical ultrasound applications. *Proceedings - IEEE Ultrasonics Symposium*, 1:227– 230, 10 2005.

[13] Xu Q. Precision motion control of piezoelectric nanopositioning stage with chattering-free adaptive sliding mode control. *IEEE Transactions on Automation Science and Engineering*, 14:1–11, 01 2016.

[14] Hossain M I, Zahid M S, Chowdhury M A, Hossain M M M, and Hossain N. Mems-based energy harvesting devices for low-power applications – a review. *Results in Engineering*, 19:101264, 2023.

[15] Habib M, Lantgios I, and Hornbostel K. A review of ceramic, polymer and composite piezoelectric materials. *Journal of Physics D: Applied Physics*, 55(42):423002, 08 2022.

[16] Xu X, Cao D, Yang H, and He M. Application of piezoelectric transducer in energy harvesting in pavement. *International Journal of Pavement Research and Technology*, 11, 09 2017.

[17] Bell A, Comyn T, and Stevenson T. Expanding the application space for piezoelectric materials. *APL Materials*, 9:010901, 01 2021.

[18] Riaz A, Sarker M, and Mohamed R. Energy harvesting from piezoelectric cantilever beam with different shapes. *International Journal of Recent Technology and Engineering (IJRTE)*, 8:1–6, 11 2019.

[19] Tian W, Ling Z, Yu W, and Shi J. A review of mems scale piezoelectric energy harvester. *Applied Sciences*, 8(4), 2018.

[20] Wang G and Lu Y. An improved lumped parameter model for a piezoelectric energy harvester in transverse vibration. *Shock and Vibration*, 2014:1–12, 02 2014.

[21] Erturk A and Inman D J. On mechanical modeling of cantilevered piezoelectric vibration energy harvesters. *Journal of Intelligent Material Systems and Structures*, 19:1311 – 1325, 2008.

[22] Karami M A and Inman D J. Electromechanical modeling of the low-frequency zigzag micro-energy harvester. *Journal of Intelligent Material Systems and Structures*, 22(3):271–282, 2011.

[23] Karami M A and Inman D J. Parametric study of zigzag microstructure for vibrational energy harvesting. *Journal of Microelectromechanical Systems*, 21(1):145–160, 2012.

[24] Karami M A. *Micro-scale and nonlinear vibrational energy harvesting*. PhD thesis, Virginia Polytechnic Institute and State University, 2011.

[25] Karami M A and Inman D J. Analytical modeling and experimental verification of the vibrations of the zigzag microstructure for energy harvesting. *Journal of Vibration and Acoustics*, 133:011002, 02 2011.

[26] Sharpes N, Abdelkefi A, and Priya S. Two-dimensional concentrated-stress low-frequency piezoelectric vibration energy harvesters. *Applied Physics Letters*, 107, 08 2015.

[27] Brewer J A. Design, modelling and fabrication of a hybrid energy harvester. Master's thesis, Massachusetts Institute of Technology, 2005.

[28] Ibrahim M. and Salehian S. Modeling, fabrication, and experimental validation of hybrid piezo-magnetostrictive and piezomagnetic energy harvesting units. *Journal of Intelligent Material Systems and Structures*, 26(10):1259–1271, 2015.

[29] Karami M A, Yardimoglu B, and Daniel I J. Coupled out of plane vibrations of spiral beams for micro-scale applications. *Journal of Sound and Vibration*, 329(26):5584–5599, 2010.

[30] Dejene N D and Lemu H G. Current status and challenges of powder bed fusion-based metal additive manufacturing: Literature review. *Metals*, 13(2), 2023.

[31] Dilberoglu U M, Gharehpapagh B, Yaman U, and Dolen M. The role of additive manufacturing in the era of industry 4.0. *Procedia Manufacturing*, 11:545–554, 2017.

27th International Conference on Flexible Automation and Intelligent Manufacturing, FAIM2017, 27-30 June 2017, Modena, Italy.

[32] Riaz A, Yuan Z, and Hohan B. Precision machining by dicing blades: A systematic review. *Machines*, 11, 02 2023.

[33] Nichiwak. `https://www.nichiwak.co.jp/english/technology/`. Accessed: 15 October 2023.

[34] Wevolver.com. `https://www.wevolver.com/article/the-ultimate-guide-to-wafer-dicing-techniques-challenges-and-innovations`. Accessed: 15 October 2023.

[35] Piezo.com. `https://piezo.com/pages/piezo-material`. Accessed: 15 October 2023.

[36] Zhou N, Li R, Ao H, Zhang C, and Jiang H. Piezoelectric performance of a symmetrical ring-shaped piezoelectric energy harvester using pzt-5h under a temperature gradient. *Micromachines*, 11(7), 2020.

[37] Techsteel. `https://www.techsteel.net/alloy/stainless-steel/17-4ph`. Accessed: 15 October 2023.

[38] EOS. `https://www.eos.info/03_system-related-assets/material-related-contents/metal-materials-and-examples/metal-material-datasheet/stainlesssteel/material_datasheet_industryline_17-4ph_m290_en_screen.pdf`. Accessed: 16 October 2023.

[39] Atimaterials. `https://www.atimaterials.com/Products/Documents/datasheets/stainless-specialty-steel/precipitationhardening/ati_17-4_tds_en_v2.pdf`. Accessed: 15 October 2023.

[40] Chew T S. Avoiding epic fails in mems microphones what you need to know about microphone arrays. *White Paper*, 2017.

[41] Ibrahim M. Design, modelling and fabrication of a hybrid energy harvester. Master's thesis, University of Waterloo, 2014.

[42] Tech-Labs. `https://tech-labs.com/products/am400`. Accessed: 15 October 2023.

[43] MSAM. `https://msam.uwaterloo.ca/infrastructure/`. Accessed: 15 October 2023.

[44] AMS F Corrosion and Heat Resistant Alloys Committee. *Steel, Corrosion-Resistant, Investment Castings 16Cr - 4.1Ni - 0.28Cb - 3.2Cu Homogenization and Solution Heat Treated or Homogenization, Solution, and Precipitation Heat Treated*, nov 2022.

[45] Bath D. Low-frequency piezoelectric energy harvester with novel 3d folded zigzag design and high power density. Master's thesis, University of Waterloo, 2018.

[46] TMS. `https://www.modalshop.com/vibration-test/products/vibration-test-shakers/75-lbf-exciter`. Accessed: 25 October 2023.

[47] PCBPiezotronics. `https://www.pcb.com/products?model=352a24`. Accessed: 25 October 2023.

[48] Suaprasert P, Aungkavattana P, and Bintachitt P. Study of the factors affecting the mechanical, electrical, and piezoelectric properties of pzt micro-actuator. *Ferroelectrics*, 459, 01 2014.

[49] Inman D J. *Engineering Vibration*. Pearson Prentice Hall, 2008.

[50] Siemens. `https://community.sw.siemens.com/s/article/how-to-calculate-damping-from-a-frf`. Accessed: 27 November 2023.

[51] Liang H, Hao G, and Olszewski O Z. A review on vibration-based piezoelectric energy harvesting from the aspect of compliant mechanisms. *Sensors and Actuators A: Physical*, 331:112743, 2021.

[52] Beeby S P, Torah R N, Tudor M J, Glynne-Jones P, O'Donnell T, Saha C, and Roy S. A micro electromagnetic generator for vibration energy harvesting. *Journal of Micromechanics and Microengineering*, 17:1257 – 1265, 2007.

[53] Roundy S and Wright P K. A piezoelectric vibration based generator for wireless electronics. *Smart Materials and Structures*, 13(5):1131, aug 2004.

[54] CAMJ. Wire bonding equipment, Oct 2023. Accessed: 25 October 2023.